EVALUATION OF PHENOTYPING METHODS FOR MAIZE

BY

ROBERT JAMES REIS

THESIS

Submitted in partial fulfillment of the requirements
for the degree of Master of Science in Agricultural and Biological Engineering
in the Graduate College of the
University of Illinois at Urbana-Champaign, 2013

Urbana, Illinois

Advisor:

Associate Professor Tony E. Grift

Abstract

The quantitative measurement of plant features, also known as “phenotyping”, is an important step in the development of improved varieties of corn. These improvements typical consist of increased yield, but also increased resistance to biotic and abiotic stresses is paramount. The speed of this crop improvement is currently limited by rather archaic methods of phenotyping, often consisting of manual measurements of morphological features. In this research, a new addition to the technology of phenotyping was developed. Earlier, image based high-throughput phenotyping methods have been developed that allow for the measurement of root complexity, stalk diameter and root angle. The method used is direct imaging of the root structures under controlled diffuse lighting. The method as developed in this work, differs in that the lighting is not diffuse, but structured in the form of a laser sheet that is projected through a root system, where the illuminated areas are recorded using a digital camera. By moving the laser sheet to vertically different areas of the root structure were illuminated. The root was also rotated, allowing for several sides of the root to be scanned and the resulting angle to be based on multiple views of the root. The same procedure was applied to tassels. The imagery was analyzed to obtain root angles that were compared to root angles measured using the direct imaging method.

Important issues for future development were identified, including sample preparation procedures, the requirements of all systems, and improvements to the technology.

To my family

ACKNOWLEDGEMENTS

This research would not have been possible without the assistance of many people. I would like to offer my appreciation to those who have educated, inspired, and aided me in this process.

First, I am extremely grateful to my advisor, Dr. Tony Grift, for his expert guidance and inspiration. This research would not have been possible without his support and direction. I would also like to thank my committee members, Dr. Martin Bohn and Mr. Stephen Zahos for their help and many suggestions to improve this thesis. I wish we could have had more interactions in order to accomplish more with this research. I would also like to thank Dr. Boris Odintsov for his help with the Magnetic Resonance Imaging and Dr. Wawrzyniec Dobrucki and Dr. Iwona Dobrucka for their help with the Computer Tomography sections of this thesis.

My sincere gratitude also goes to my friends and colleagues, Dr. Lei Zhang, Dr. Sunil Mathanker, Dr. Zewei Miao, Mr. Fu Ouyang, Mr. William Roy, Ms. Wei Zhao, and Mr. Hao Gan for their assistance, cooperation, and friendship. I thoroughly enjoyed working with them and appreciate the assistance and friendship they provided.

Last but not least, I am forever indebted to my parents. Their love, understanding and encouragement are invaluable and are responsible for making me the man I am today.

TABLE OF CONTENTS

LIST OF ACRONYMS

USDA	United States Department of Agriculture
NASS	Nation Agricultural Statistics Service
NASS	National Agricultural Statistics Service
UIUC	University of Illinois at Urbana-Champaign
CS	Crop Sciences
ABE	Agricultural and Biological Engineering
DNA	Deoxyribonucleic acid
CT	Computer Tomography
MRI	Magnetic Resonance Imaging
CRIB	Corn Root Imaging Box
LSCRIB	Laser Sheet Corn Root Imaging Box

CHAPTER 1

INTRODUCTION

Corn is an extremely important component of agriculture in the United States, with production values reaching $77 billion in 2012 (USDA-NASS, 2013). Crop scientists continually try to increase yield by selective breeding. An important step of this selective breeding process is the measurement of physical parameters of plant varieties, a practice known as phenotyping. Phenotyping relies heavily on skilled technicians performing manual measurements and data entry, making human labor a major cost of developing new crop varieties. Therefore, reducing personnel expense by increasing the speed with which samples can be phenotyped would be a significant benefit to plant breeders. Also human biases are eliminated, increasing the accuracy of measurements. To accomplish this, the concept of laser sheet imaging was pursued to determine root angle of corn plants. This system consisted of 1) a Corn Root Imaging Box (CRIB), 2) a mobile laser sheet system to illuminate the area being measured, and 3) a camera to record the data. This thesis describes the development of such a rapid phenotyping machine termed the Laser Sheet Corn Root Imaging Box (LSCRIB), including the hardware and software needed to effectively measure length parameters in corn roots.

1.1. Research Motivations

Corn (Z. mays) is an extremely important crop in the United States with a production value of 10.7 billion bushels, worth $ 77 billion in 2012. (USDA-NASS, 2013). Corn originated in the Americas and was in use as a food crop prior to the arrival of Europeans (Crabb, 1992). It has many uses; including livestock feed, fuel ethanol, and multiple food products.

According to the most recent United Nations projection, the current world population is 7 billion people and is expected to grow to 10.1 billion people by 2100. To feed this increasing population, crop yields must be increased dramatically. This need for increased agricultural productivity has occurred in the past; during the Green Revolution era, a time period between the 1940s and the 1970s, the world food output (particularly in India, Pakistan and Mexico) was dramatically increased by utilizing modern agricultural techniques (Parayil, 2003) and the development of semi-dwarf, high-yield, disease-resistant wheat varieties. In order to feed an ever increasing population, a second Green Revolution is needed. Historically, a prime driver for increasing crop yield has been advances in crop breeding. This can clearly be seen in the United States historical corn yields shown in figure 1. In this case, yield improvements shown by the inflection points of 1937 and 1996 were driven primarily by the adoption of hybrid corn and transgenic hybrid corn. This has increased the annual rate of yield improvement from approximately 0 kg/ha/year (0 bu/ac/year) prior to 1937 to 125 kg/ha/year (2.0 bu/ac/year) after 1996.

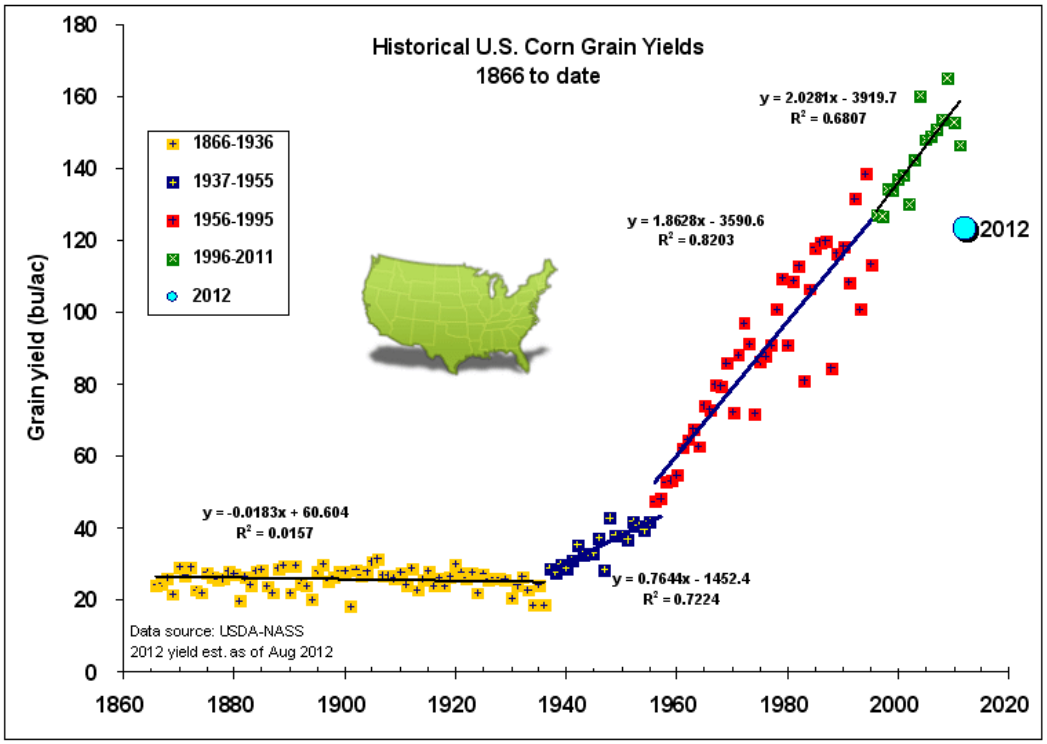

Figure 1: Historical US corn grain yields from 1866-date. From: http://www.agry.purdue.edu/ext/corn/news/timeless/YieldTrends.html accessed, 11/27/2013.

To continue improvement of crop yields, research is conducted to develop new varieties of high yielding corn plants. Researchers now link genetic data of individual plants to phenotypic data. Recent advances in DNA marker assays and sequencing have dramatically decreased the cost and time needed to obtain genotypic data (Peleman and Van Der Voort, 2003). However, the speed with which corresponding statistically significant phenotypic data can be acquired has not increased at the same rate and has become a bottleneck in the development of new crop varieties. This step, (known as phenotyping) is currently done by skilled technicians using labor intensive manual measurement techniques. The data is then recorded manually into a spreadsheet, allowing for the possibility of data entry errors. This practice is expensive and time consuming as many samples must be processed to obtain a statistically significant data set. For example,

approximately half of the corn ear samples waiting for phenotyping by researchers involved in this project prior to the start of this project can be seen in figure 2. Some alternatives have been adopted with unsatisfying results; thus, a more advanced solution is desired to address this issue.

Figure 2: Sacks containing about 3,000 corn ears, ready to be phenotyped.

Researchers at the University of Illinois at Urbana-Champaign (UIUC) department of Crop Sciences (CS) and the department of Agricultural and Biological Engineering (ABE) collaborated on the development of such a phenotyping system. The apparatus was built by the ABE department and tested using samples from the CS department. The same samples were then measured using the current manual methods to validate the data generated by the new apparatus.

1.2. Objectives

The goal of this project being the development of an automated phenotyping system is ambitious and requires cooperation from researchers in several fields. The work necessary to accomplish this goal was comprised of the following three objectives.

(1) Construction of a phenotyping system

(2) Testing of samples

(3) Validation of samples using current techniques

CHAPTER 2

LITERATURE REVIEW

Section 2.1 discusses advanced 3D scanner applications. Section 2.2 discusses advanced visualization techniques not reliant on the visual spectrum. To illustrate both classical and modern methods used for phenotyping, section 2.3 discusses the history of plant breeding and section 2.4 discusses current techniques used in phenotyping. Section 2.5, discusses advanced sensor system applications in agriculture. Finally section 2.6 describes advanced techniques for high throughput phenotyping.

2.1 Advanced 3D Scanner Applications

Environment modeling and object scanning are the two primary applications of 3D scanners (Se and Jasiobedzki, 2006). Its ability to quickly and inexpensively provide depth perception has caused its recent adoption into many applications including mobile robotics, construction, and forensics.

Mobile robots require 3D information about its environment for navigation and task planning. Tamas and Goron (2012) developed a 3D laser scanner system and used it for robot navigation in several environments. Here the laser system was developed from a commercial 2D system placed in a custom rotary platform to gain an additional third degree of freedom. Roh et al. (2013) developed a method for simultaneously localizing and mapping objects for mobile robot navigation. Often, the information from 3D scanners is combined with other sensors to

provide synergistic data. Osswald et al. (2012) combined a laser scanner system and an inertial measurement system with joint encoders to allow a humanoid robot to determine its pose for climbing stairs. Freitas et al. (2012) developed an obstacle avoidance system for robot navigation in an orchard. This system uses a laser scanner, low-cost inertial measurement unit, and encoders in the wheels and steering system to detect and navigate around obstacles.

Laser scanners are also commonly used in the construction industry. The scanners produce 3D models commonly known as building information models (BIMs). Xiong et al. (2013) developed a method to automatically convert raw 3D point data from multiple scans into BIMs. Brenner and Ripperda (2008) developed several methods to orient terrestrial laser scans without the use of artificial targets. These scanners are used throughout the lifecycle of a structure, from planning (Tang and Akinci, 2012) and construction (Turkan et al., 2013) to facility maintenance (Tang and Burcu, 2012) and have even been used to preserve architectural heritage sites (Núñez Andrés and Buill Pozuelo 2008; Kersten and Lindstaedt, 2012).

Forensics has also found many uses for 3D laser scanners. Historically, sketches and photographs from investigators have been used to record crime scenes at the time of discovery. However, these are 2D methods, limiting their usefulness. 3D laser scanners have recently been applied to mapping crime scenes (Komer et al., 2011) where their ability to gather depth information has proved highly valuable. 3D laser scanners have also been applied to modeling human remains (Santamaría et al., 2011; Sholts et al., 2010). Here the ability to quickly record measurements of remains without the need for skilled sketch artists has sped up the work of medical examiners.

2.2 Advanced Visualization Techniques Not Reliant on the Visual Spectrum

Several methods have been developed to produce 3D images using non-optical technologies. These techniques were developed to produce images noninvasively and have found applications in medicine, structural health monitoring, and quality control. Section 2.2.1 describes ultrasonic imaging. Section 2.2.2 describes computer tomography. Section 2.2.3 describes magnetic resonance imaging.

2.2.1 Ultrasonic Imaging

While investigations of inaudible sound waves date back to the 19th century, modern ultrasonic research began around 1917 for use in the detection of submarines. This work built on the advances in electro-acoustics made in the 19th century (Mason, 1964). Soon other uses of ultrasonic imaging were found including medical imaging (Newman and Rozycki, 1998), seismic analysis, and ultrasonic inspection (Berkhout, 1989).

Ultrasonic imaging consists of illuminating the sample with high frequency acoustic waves and deriving information about the mechanical properties of the interior of the sample from the reflected wave field. The differences in the reflected wave-field are due to varying acoustic properties of materials contained within the sample. These differences are due primarily to variations in the modulus of elasticity of the materials (Berkhout, 1989).

2.2.2 Computer Tomography

Computer Tomography (CT) is another advanced technique for visualizing objects noninvasively. Unlike traditional x-ray imaging, CT allows for objects to be imaged in three dimensions. While ideas for reconstructing images from multiple projections date back to 1940, the first CT scanner was built in 1963 by Allan Cormack (Hsieh, 2009). CT has found applications in medicine (Cierniak, 2011), engineering, and geoscience (Mees et al., 2003).

CT relies on x-ray flux measurements from different angles to form an image. Each angle produces a measurement fundamentally identical to that created by a conventional x-ray detector after attenuation by a patient. The logarithm of the ratio of the input x-ray intensity to the output x-ray intensity represents the line integral of the attenuation coefficients along the x-ray path. These attenuation coefficients of materials to x-rays are known. Therefore, under ideal conditions, the reconstruction problem in CT is using measured line integrals of an object in order to calculate attenuation distributions within that object. This essentially forms parallel 2D images, which are used in reconstruction of a 3D image (Hsieh, 2009).

Recent advances in CT have increased the precision and acquisition speed of CT scans. The first generations of devices were equipped with a pencil beam and a single detector. However, by equipping the devices with a cone shaped beam (now usually between 40 degrees and 60 degrees) and a detector ring, acquisition speed has been increased (Buzug, 2008). Another advanced application of CT is micro-CT – essentially a miniaturized cone-beam CT for a very small volume. This technique is commonly used for materials testing, particularly in viewing composite materials (Batranin et al., 2013). Another advanced imaging technique using CT is a positron emission tomography (PET)-CT scan. This technique is used in medicine to

study metabolism. A patient is injected with a radioactive tracer that can be metabolized inside the body. Cells which metabolize faster (such as cancer cells) appear brighter than other cells in a PET scan. By combining PET with CT, the fast metabolizing cells appear as bright spots in relation to the remaining cells, whose locations and compositions are determined by CT (Basu and Alavi, 2011).

2.2.3 Magnetic Resonance Imaging

Another technique that uses radiation to image objects noninvasively is magnetic resonance imaging (MRI). The first MRI machine was developed by Raymond Damadian at the State University of New York in 1972. However, this device was unable to generate images. Later, Paul Lauterbur of the University of Illinois (Lauterbur, 1973) and Sir Peter Mansfield of the University of Nottingham (Schwarzschild, 2003) expanded on earlier work to produce images from such scans. For this, they both received the Nobel Prize for Physiology or Medicine in 2003.

MRI relies on the nuclear magnetic resonance property of water inside of the sample for imaging. The average magnetic moment of protons within the water molecules are aligned in a large magnetic field. Then a radio frequency current is turned on at the resonance frequency of the sample, which flips the spin of the protons within the magnetic field. After this radio frequency is turned off, the protons spin returns to an equilibrium which causes a radio frequency signal to be emitted. This radiation is detected by receiver coils (Mansfield and Pykett, 1978).

MRI is primarily used for medical imaging. One important area of MRI advancement is in the area of contrast agents. Unlike contrast agents in x-ray based imaging techniques, MRI

contrast agents are not visible. Instead, they interact with the protons by either modifying their relaxation times or are involved in the level of proton magnetization. Other advances involve creating a pulse sequence optimized to provide contrast based on the object being investigated (Merbach et al., 2013).

2.3 The History of Plant Breeding

Archeological records have shown that crops were domesticated some 10,000 years ago in the Fertile Crescent region, the land surrounding the Tigris and Euphrates rivers (Zeder, 2011). Since the beginning of agriculture, farmers have selectively bred crops in an attempt to increase yields. Early selective plant breeding relied on three distinct processes. First, the breeders made purposeful, unremitting selections. Second, the selections were widely propagated. Lastly, hybridization of plant varieties with desired traits was performed to create offspring with traits from both parents (Ulukan, 2009). Records of targeted plant breeding programs date back to at least 700 BC, when the Babylonians and Assyrians recorded artificially pollinating palm trees (Hulse, 2004). This process was refined over time, resulting in progressively greater yields.

More recently, the use of genetic engineering in plant breeding has allowed an even greater rate of crop optimization for human use (Jauhar, 2001). The use of high-throughput genomic technologies such as DNA marker assays (Peleman and Van Der Voort, 2003), microarrays and next-generation sequencing (Pérez-de-Castro et al., 2012), and marker-assisted selection (Ophir, 2013) were prime drivers for this phenomenon and yielded great increases in agricultural production. Both classical and modern plant breeding have yielded dramatic advances in productivity. For example despite a relatively consistent acreage devoted to US corn

production, yield has gone up by a factor of nearly 6 since 1925 as shown in figure 3. Still, environmental conditions can cause major deviations from the expected mean yields, as evidenced by a decrease in yield measuring 23% in the drought year 2012, compared to the record yield of 10 Mg/ha (160 bu/ac) set in 2010.

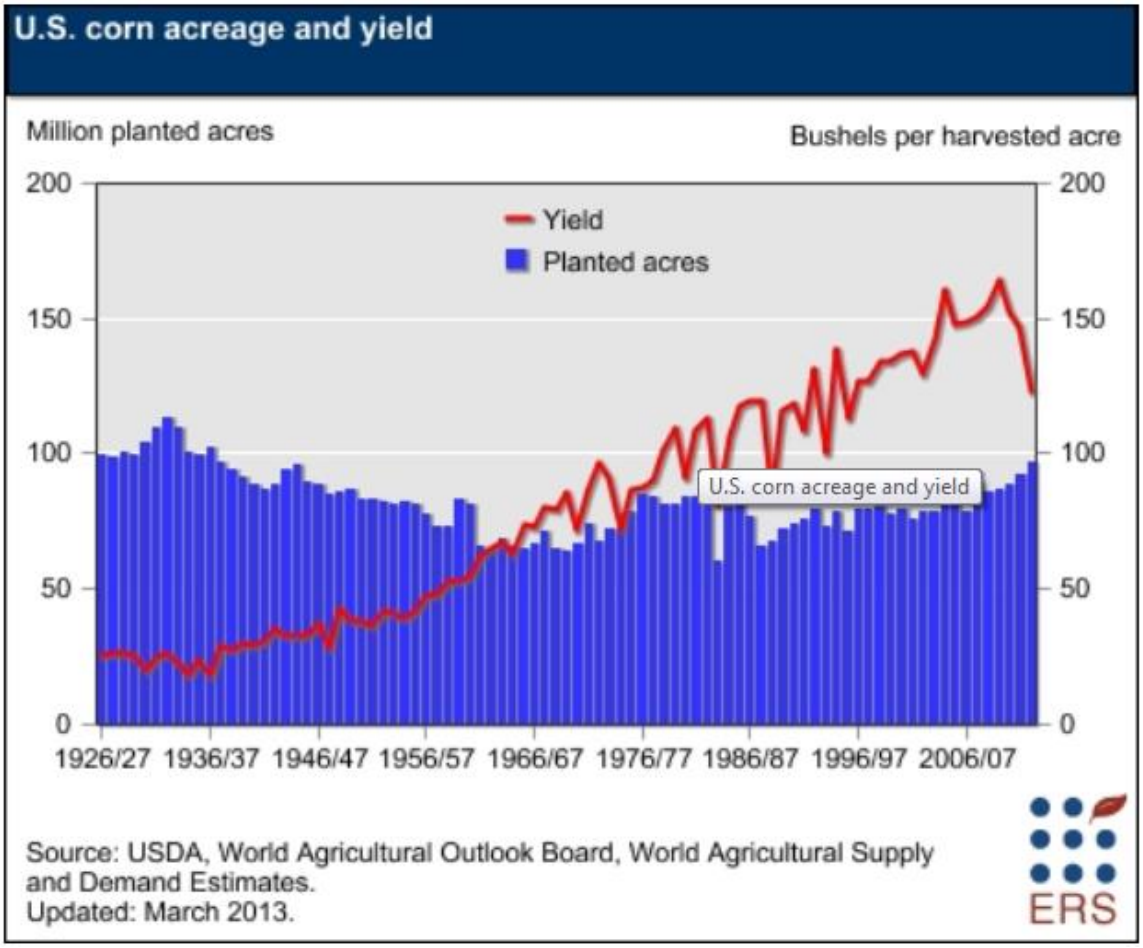

Figure 3: Yield trends and planted acreage of US corn from 1926-2012. Notice the increasing variability in the 1966-2012 era, and the effect of drought in 2012 (final datapoint). From http://www.ers.usda.gov/topics/crops/corn/background.aspx#.UXoLBqLql8E, accessed 11/27/2013.

2.4 Current Methods for Phenotyping.

While the rate at which crop genetic data can be measured has increased exponentially in recent years (Vaughan et al., 2007), the rate at which a statistically significant sample set of phenotypic data can be acquired has increased at a much slower rate. This is due primarily to the manual measurement techniques utilized in this process. For example, length parameters are measured using rulers and weight measurements are taken using a digital scale. Examples of such equipment used for these measurements can be seen in figures 4 and 5

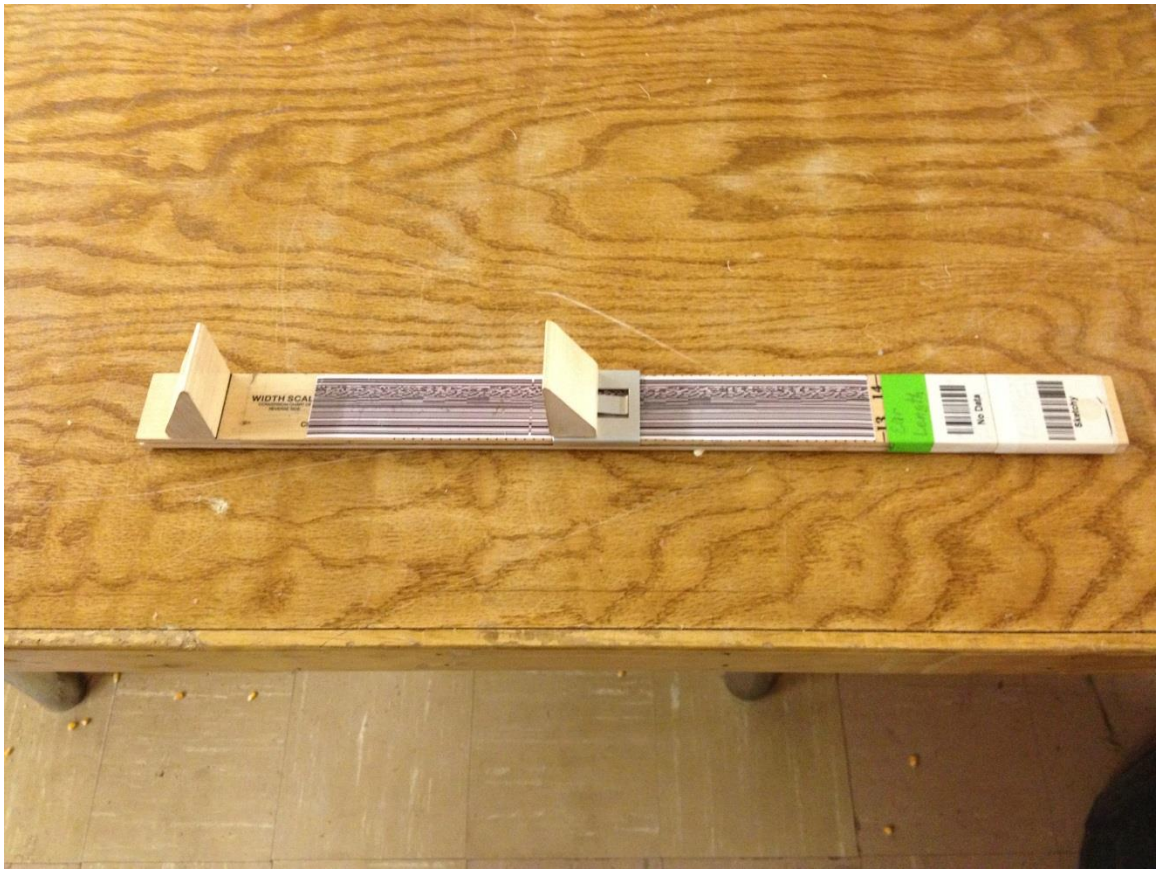

Figure 4: Tool for measuring the lengths of corn ears. The length of the ear can be obtained using a barcode reader, which decreases the chance of measurement error.

Figure 5: Typical tools used for manual phenotyping. These tools require ample manual labor. To increase the throughput, these tools need to be replaced by automated machinery.

Additional important plant characteristics are measured manually. For instance, Trachsel et al. (2010) were able to manually characterize architectural traits of corn roots in the field and characterize the variability between samples using protractors. Koc et al. (2012) used liquid chromatography and electrospray time-of-flight mass spectrometry to profile relatively low-molecular weight proteins in varieties of corn. These measurements require significant time from a trained technician, resulting in high expense for processing the large sample sizes needed.

2.5 Advanced Sensor Systems in Agriculture

Sensor systems have been used in agricultural applications for many years. However, recent advances in precision agriculture as well as the desire to maximize yields with minimum cost have caused widespread adoption of advanced sensor systems. Section 2.4.1 discusses recent developments in pre-harvest sensor systems. Section 2.4.2 discusses recent developments in post-harvest sensor systems.

2.5.1 Pre-Harvest Sensor Systems

To maximize yields, crops must be protected from both abiotic stresses (such as water and nutrient stresses) and biotic stresses (such as diseases, insects and competition from weeds) (Grift et al., 2008). Precision agricultural techniques have been applied to minimize these stresses as efficiently as possible. These techniques require utilization of advanced sensor systems.

Significant research has been devoted to monitoring abiotic stresses, a vital component of monitoring plant health. This includes soil parameters such as macro-nutrient levels, soil compaction, and moisture level. Understanding the soil conditions at specific points in the field allows for more efficient crop protection and management, ultimately increasing yields and decreasing costs (Sinfield et al., 2010). Ehsani et al. (1999) developed a technique to rapidly determine soil mineral nitrogen content using near-infrared reflectance. Hak-Jin et al. (2007) developed a method to measure nitrogen, potassium, and phosphorus levels in soils using ion-selective electrodes. Grift et al. (2005) characterized soil compaction layers by measuring the acoustic interaction caused by a cone drawn through soil. Andrade et al. (2004) used an array of

load cells to characterize soil compaction layers. Adamchuk et al. (2001) developed a strain gauge array to dynamically measure soil mechanical impedance. Garbout et al. (2013) used a 3D CT scan to measure morphometric parameters of soil under varying tillage conditions.

Monitoring biotic stresses is also an important area of research in crop health monitoring. One such parameter that is extremely important in agriculture is weed proliferation. Camera systems have been commonly used for this purpose, primarily using two techniques: crop line identification (where all plants not in the crop line are considered weeds) and weed identification by physical properties of the individual weeds (Grift et al., 2008). Zhang and Chaisattapagon (1995) were able to characterize color and shape properties for several common weed types. This technique has been optimized for use with many commercially significant plants including soybean, (Tian, 2002; Samseemoung et al., 2012), corn (Romeo et al., 2013), and cotton (Sui et al., 2008).

Monitoring crop disease is important to minimize crop loss. The earlier these diseases are found, the more effectively and efficiently they can be treated, reducing both crop loss and the amount of chemical treatment needed. Traditionally, detection of crop disease has relied upon manual inspection of fields. However, advances in sensors have allowed researchers to develop methods to rapidly detect bacterial and viral illnesses. Significant work has been done in optical sensing, since most plant infections result in changes in the optical reflectance of leaf surfaces. Optical sensors have been used to detect several illnesses including huanglongbing in orange trees (Garcia-Ruiz. al, 2013), cercospora leaf spot, sugar beet rust and powdery mildew in sugar beet (Mahlein et al. 2013), and yellow rust in winter wheat (Byson et al. 1997). Olfactory sensors have also been used for identifying crop diseases. Blasioli et al. (2010) used an electronic nose to detect crown gall illness in grapevines. Zhou and Wang (2011) utilized an electronic nose to

discriminate among types of damage incurred by rice plants. Huang et al. (2011) were able to determine the flowering stage of Cymbidium ensifolium (a type of ornamental flower) using an electronic nose. Jiang et al. (2012) developed a method to inspect wheat tiller using CT.

2.5.2 Post-Harvest Sensor Systems

Advanced sensor systems have also been applied post-harvest to insure product quality and safety. Vision systems have been utilized to evaluate crops based on size, shape, color, freshness condition, and the presence of visual defects (Costa et al., 2011). These techniques have been applied to many crop varieties after harvest including fresh-cut potato (ElMasry et al., 2012), starfruit (Abdullah et. al., 2006), apple (Leemans and Destain, 1998), and wheat (Manickavasagan et al., 2008). Often, many properties are used for evaluation at once. Liming and Yanchao (2010) developed a method to grade strawberries based on shape, size, and color. Majumdar and Jayas (2000) developed a method to classify cereal grains using machine vision based on morphology, color, and texture of the kernels.

Characterizing the chemical composition of crops post-harvest is also an important application of advanced sensor systems and has applications for quality control and consumer safety. Molina et al. (2013) were able to rapidly characterize corn grain by photo-acoustic spectroscopy. Near infrared spectroscopy has been applied to many food sources including wine (Cozzolino et al., 2005), carrot (De et al. 2003), pea (Martens and Martens, 1986), olive oil (Kapoulas and Andrikopoulos, 1987) and rice (Delwiche et al., 1996). Fang et al. (2013) were able to rapidly characterize various oils and animal fats using proton nuclear magnetic resonance and chromatography-mass spectrometry. Koizumi et al. (1996) developed a dedicated MRI

apparatus for use in quality inspection of foods. It allows for analysis of distribution patterns of fats within meat, as oil-accumulating tissues in plants, as well as the analysis of the vasculature in plants. Others have used MRI to inspect olive oil (Dais and Hatzakis, 2013, Mannina and Sobolev, 2011) and apple (Clark et al., 1998). Another method used to evaluate product quality post-harvest is CT, a technique that allows for examination of internal structures of the subject. It has been used to study peach (Barcelon et al. 1999), mango (Kotwaliwale et al. 2012) and wood logs (Longuetaud et al., 2004 and Yu and Qi, 2008).

Korostynska et al. (2013) were able to verify vegetable oil types using microwave sensors. Others have focused their efforts on the use of olfactory sensors. González et al. (1999) were able to differentiate between types of vegetable oils using an electronic nose. Yoshida et al. (2012) used an electronic nose to detect rancidity for quality purposes in several types of nut. Hernández et al. (2007) were able to correlate smell (detected using an electronic nose) with fruit ripeness for harvested mandarin. Zhang and Wang (2007) were able to determine the age and degree of insect damage in stored wheat using an electronic nose.

2.6 Rapid Phenotyping Techniques

Phenotyping is currently the bottleneck in the process to characterize genetic factors that contribute to variations in the physical characteristics of crops (Cobb et al., 2013). The theory of constraints (Goldratt, 1990) also identifies this step as the bottleneck in the process of linking genetic data to phenotypic data due to the presence of large quantities of work-in-progress (WIP) inventory (i.e. samples waiting to be phenotyped) prior to this step. This WIP arrives in the phenotyping lab in extremely large batch sizes (typically all are harvested at once), further

compounding this problem. Goldratt's theory of constraints finds that addressing the bottleneck is the most efficient method for increasing throughput in a process. This can be accomplished either by increasing the current type of resources used (i.e. increasing the number of technicians performing manual measurements) or by acquiring more efficient resources. Several methods have been developed to increase the efficiency of tools used for phenotyping. Section 2.6.1 addresses techniques developed for rapid phenotyping that use digital image processing. Section 2.6.2 addresses techniques developed for rapid phenotyping that use other methods.

2.6.1 Rapid Phenotyping Using Digital Image Processing

Digital image analysis has provided new opportunities for researchers to rapidly study physiological characteristics of plants. One area of particular interest has been studying the root structures of plants (Zhu et al., 2011). Grift et al. (2011) used the fractal dimension of images of corn roots to characterize the complexity of the root structure. Grift and Bohn. (2013) developed a Corn Root Imaging Box (CRIB) to obtain highly detailed images of corn roots to measure root complexity, root angle, and stem diameter. Clark et al. (2013) developed a two-dimensional root system phenotyping platform and corresponding software. They then applied the technique to the root structures of several crop species. Armengaud et al (2009) also developed a software package to scan roots using a two-dimensional method. This method relies on growing the plants in a vertical Petri dish of clear agar prior to acquiring the images. Three dimensional imaging has also been conducted. Basu and Pal (2009) developed a method to take a time lapsed series of two-dimensional images to develop a three-dimensional image of the root structure. In situ three-dimensional imaging of root structures has also been explored. Fang et al. (2009) used a laser

scanner to image rice roots in a solid gel matrix. X-ray computed tomography was used by Mooney et al. (2006) to study soil and root structure in cereal crops under various soil conditions. Neethirajan et al. (2008) used computer tomography to analyze the geometry of wheat and pea pores.

Digital image processing has been applied to yield estimation of crops. Yi et al. (2008) used airborne hyper-spectral imagery to develop yield prediction methods for individual citrus trees. Several of the techniques developed for estimating miscanthus giganteus yields by Zhang and Grift (2012b) relied on images produced either with a laser sheet angled relative to a camera or with two cameras. Lee and Lee (2013) used analysis of color images of rice fields for yield prediction and crop management.

Often parameters that must be measured in phenotyping require counting large quantities of material. When performed manually, this can be tedious, error prone, and time consuming. Techniques in digital image processing have been applied to solve this problem. Severini et al. (2011) applied open source software to digital photographs of dispersed corn kernel samples to rapidly acquire an accurate kernel count. Liu et al. (2012) developed a method to count kernels on an ear of corn. Digital image analysis has also been applied to counting pollen grains (Costa and Yang, 2009). They found that applying digital imaging and image processing both reduced labor costs and reduced the chance of error.

Digital image analysis has also been applied to measuring other crop parameters. Romano et al. (2011) used thermal imaging of corn fields to determine crop tolerance to water stress. Here, a correlation between crop temperature and the ability of a genotype to adapt to water stress was determined. Lelong et al. (1998) used hyper-spectral imaging of wheat to

determine the effects of water stress. Welle et al. (2005) developed several methods to monitor important phonotypical characteristics of corn. This technique involves near-infrared spectroscopy sensors mounted on combines to monitor physical and chemical characteristics of corn as it is harvested. In addition, a non-invasive method using spectral reflectance of the plant canopies was developed that allowed monitoring of physical and chemical characteristics of the plants as they grow. Backhaus et al. (2010) developed a phenotyping software package that allows for the analysis and comparison of leaf shapes and applied this tool to several genotypes of Arabidopsis.

2.6.2 Rapid Phenotyping Using Other methods

Other methods have also been used for rapid phenotyping. Grift and Oberti (2006) developed two methods to measure the root collar diameter of pine seedlings. These methods utilized a time-of-flight measurement system combined with a counterbalanced measurement device. LIDAR (Laser Imaging Detection and Ranging) has also been used for phenotyping. Lefsky et al. (1999) used LIDAR for imaging canopy structure and biophysical properties of Douglas-Fir Western Forests. Popescu et al. (2003) used LIDAR to measure individual tree diameters and estimating forest volume. Van der Zande et al. (2006) used LIDAR to derive a quantitative method to describe tree structures. Saeys et al. (2008) used LIDAR to estimate crop density and crop volume for small grains. Weiss and Biber used LIDAR for plant detection and mapping for autonomous agricultural robots. LIDAR was also used by Zhang and Grift (2012a) for estimating miscanthus giganteus yields.

CHAPTER 3

MATERIALS AND METHODS

This chapter elaborates on the equipment developed and techniques used in this project. Section 3.1 is devoted to describing the rapid phenotyping apparatus developed in this study. Section 3.2 describes how the samples were prepared and tested. Section 3.3 describes the methodology used for measurement of the samples. Section 3.4 describes the current phenotyping method used to validate the new apparatus. Section 3.5 describes advanced visualization techniques evaluated for potential future use in imaging agricultural materials.

3.1 Rapid Phenotyping Apparatus

At the start of this project, an industrial-grade FANUC M-16iL currently in the Robotics and Instrumentation laboratory at the UIUC ABE department was considered for use in this project. A picture of this robot can be seen in figure 6.

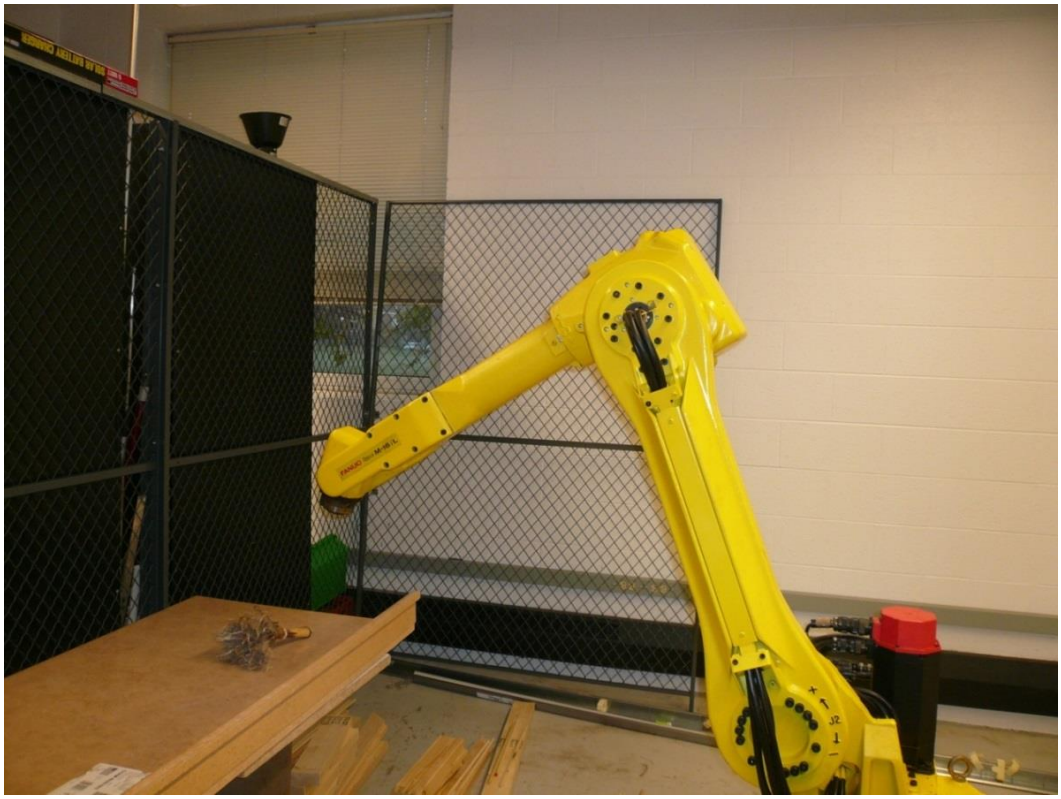

Figure 6: FANUC M-16iL industrial robotic arm. This robot was initially targeted for handling of corn roots and ears, but this method was replaced by a Corn Root Imaging Box that simplifies using structure lighting and image acquisition.

However, the desire to create a portable unit caused a shift to the use of a custom Corn Root Imaging Box (CRIB) with an attached phenotyping apparatus. This design as shown in figure 7 was completed using Solidworks® (Dassault Systèmes SolidWorks Corp., Vélizy, France).

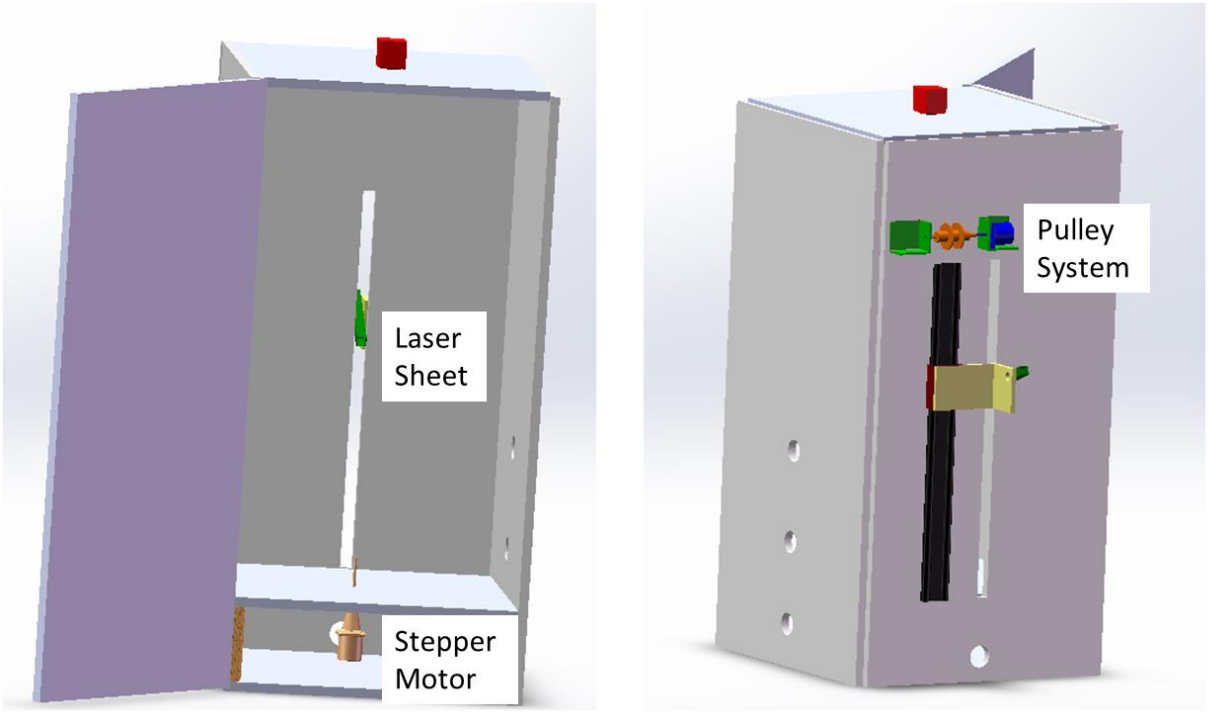

Figure 7: Left: SolidWorks(R) model of the Corn Root Imaging Box with laser lighting. The box is built around a base that contains the power supply and a stepper motor with driving hardware that allows for rotating roots and tassles. Right: The laser arrangement was placed on the back of the box, it consists of a platform mounted on a rail. A second stepper motor that is attached to a winch system allows the laser sheet generator to be moved up and down.

The hardware used for this apparatus is discussed in detail in section 3.1.1. Section 3.1.2 is dedicated to the software developed for this project. Section 3.1.3 discusses the method used to calibrate the apparatus.

3.1.1 Hardware

Section 3.1.1.1 discusses the materials used to construct the box containing all of the subsystems used for the rapid phenotyping apparatus. Section 3.1.1.2 describes the sample stand system. Section 3.1.1.3 discusses the laser sheet system and section 3.1.1.4 discusses slider system. Section 3.1.1.5 describes the camera system.

3.1.1.1 Laser Sheet Corn Root Imaging Box (LSCRIB)

The LSCRIB was made from 609.6 mm X 1219.2 mm X 19.05 mm (24 in X 48 in X 0.75 in) HDPE Material. This material was chosen for its durability and tolerance of humid environments. The HDPE boards formed the three perimeter walls and the door. The door was attached to the exterior of the LSCRIB via two hinges and a magnet. The roof and floor of the LSCRIB were made of 590.55 mm X 590.55 mm X 19.05 mm (23.25 in X 23.25 in X 0.75 in) sections of this same material. A hole of 38.1 mm in diameter was drilled into the center of the top board for mounting the camera and a hole 6.3 mm in diameter was drilled into the center of the bottom board for mounting the sample mounting stand. To facilitate the laser sheet system, a slit 19.05 mm (0.75 in) in width and 749.3 mm (29.5 in) in length was cut into the back board. This slit allowed the laser system to be raised vertically. Black cloth was placed over the top and along the back of the box to prevent ambient light from entering the imaging chamber. Black cardboard also was used to line the interior of the box to further reduce light entering the test chamber through the partially translucent HDPE material.

3. 1.1.2 Sample Stand System

The sample stand system consists of a rod 100 mm in length sharpened at one end and threaded at the other. The sharpened end of this rod was placed through the hole in the base of the bottom board. The threaded end was mounted into a wooden rectangular block with dimensions 20 mm X 20 mm X 40 mm. This wooden block was attached to a 600 mA stepper motor (JAMECO model number 57BYG084-R). This motor was powered by a 12 V power supply (TRC electronics ELN-60-12) and controlled by a Pontech® STP101 Motor Controller board connected to a computer through a serial interface (figure 8).

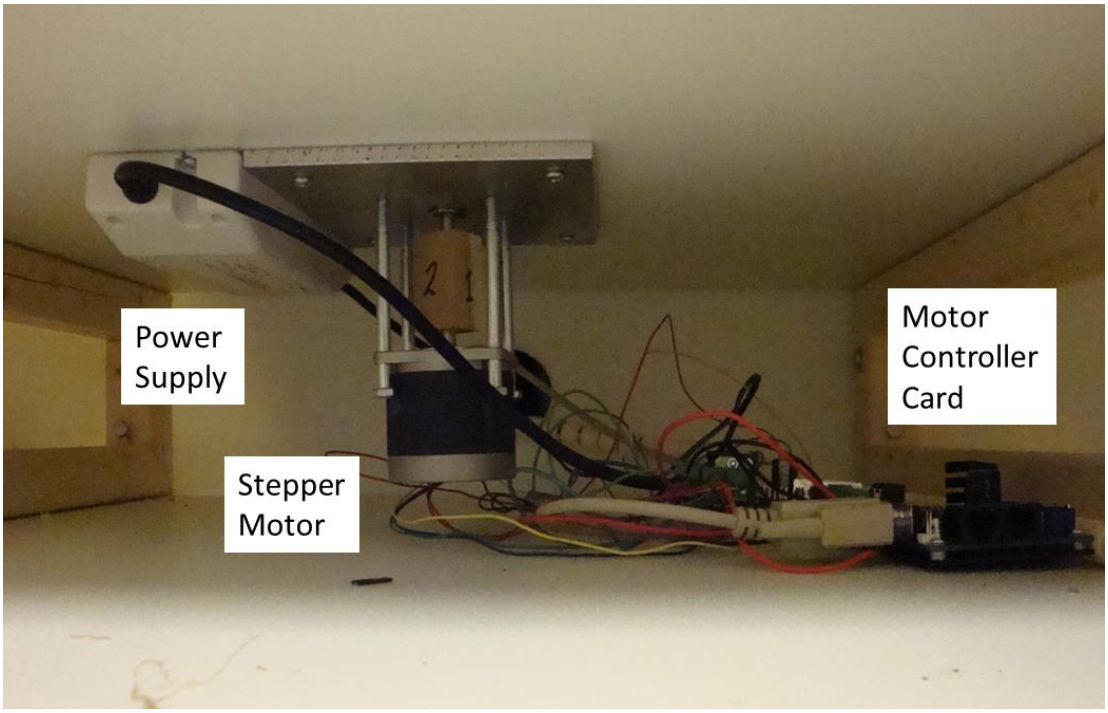

Figure 8: The Corn Root Imaging Box base show the stepper motor that is driven by a controller board, as well as the power supply mounted against the "ceiling". The stepper motor is connected to a rotating “spike” on which the roots are pinned during processing. A serial interface was used to communicate with the stepper motor drive board from a computer.

3.1.1.3 Laser Sheet System

The laser sheet system consists of a 532-nm wavelength (green) 50 mW laser, placed into a 200 mm long, rectangular section of aluminum rectangular tubing. A Fresnel lens was attached to the front of the tube and positioned in front of the laser such that it produced a laser sheet. A hole was drilled in the top of the aluminum tube and a nut was welded on top of this whole. A screw was then threaded into this nut which operated the laser. This laser sheet system was attached to a cart via custom bracket and oriented so that it was horizontal. A picture of this system can be seen in figure 9.

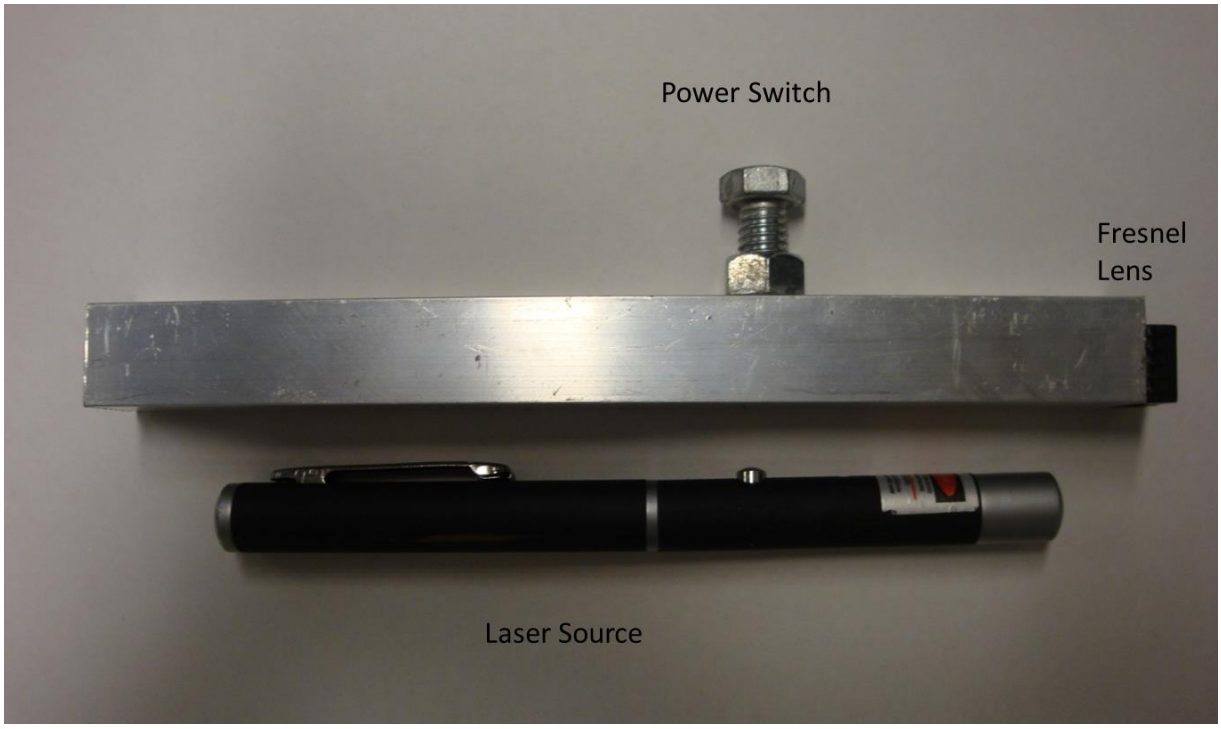

Figure 9: Laser sheet generator consisting of a 50 mW green laser, and a Fresnel lens.

However, it was discovered that the laser intensity quickly diminished as the batteries drained. Examples of the variation in laser intensity caused by rapid battery discharge are shown in figure 10.

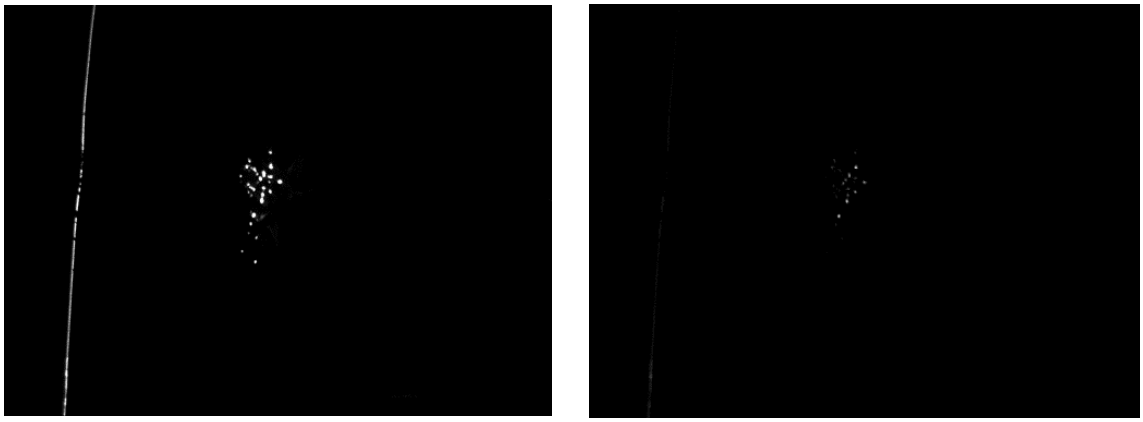

Figure 10: Left: Laser sheet interception at full battery power level. Right: same interception pattern at reduced battery power level. The battery was eventually replaced by a 3 Volt power supply.

Therefore, the battery source was replaced by a Global Specialty Industries 1310 power supply and a switch to provide 3 V DC to the laser source. This system can be seen in figure 11.

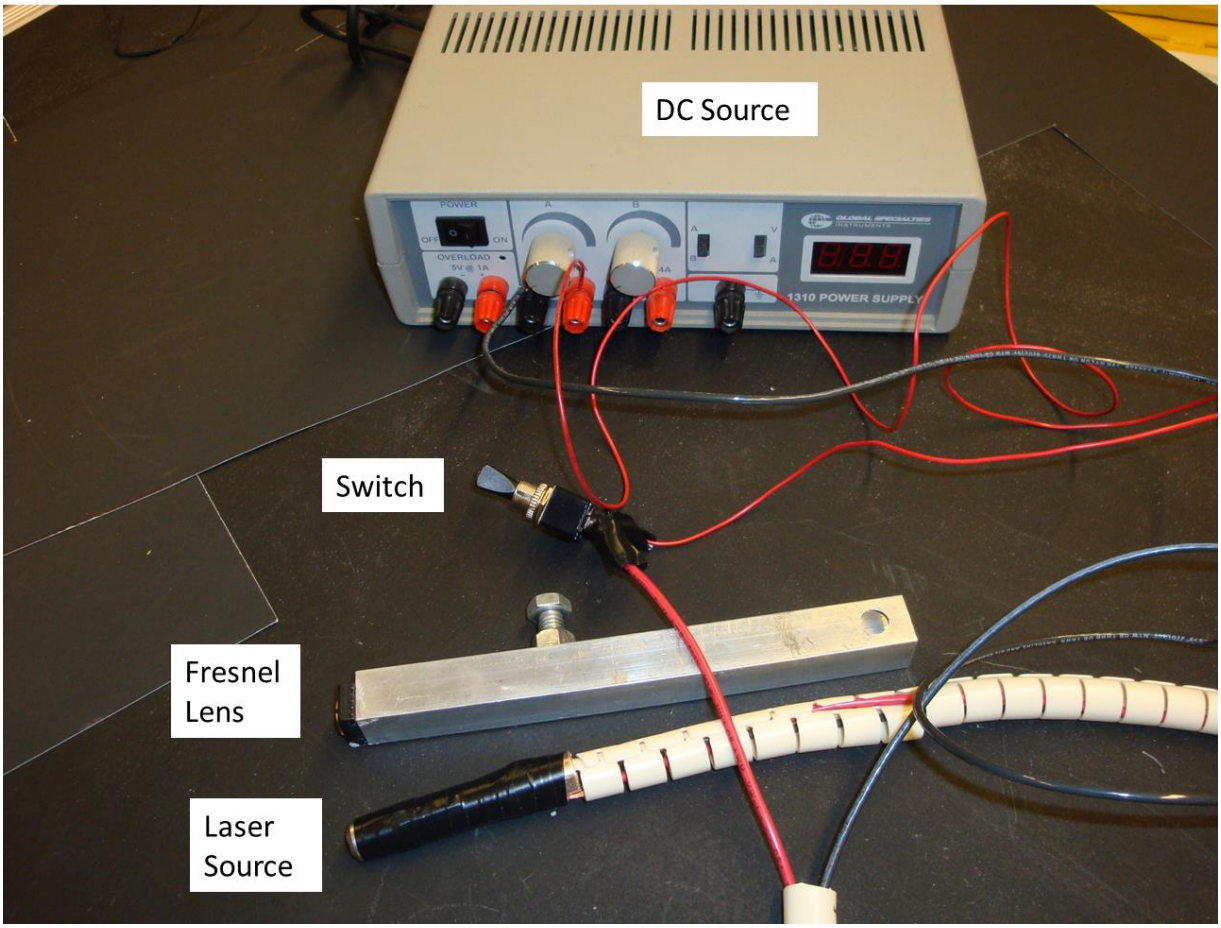

Figure 11: The laser sheet was generated using a laser pointer source (532 nm, green) powered by a 3 V power supply and manually switched on and off.

3.1.1.4 Slider System

The laser sheet assembly was attached via a custom bracket to a slider on a 30 inch section of Igus DryLinW1040-A linear guide camera slider. Above this slider, a custom motorized winch system was mounted consisting of 12 V, 600 mA stepper motor (JAMECO model number 57BYG084-R), a driven pulley, and two custom mounting brackets. The motor was connected to a computer via a Pontech® STP101 Motor Controller card located in the base of the apparatus. The motor was attached to the slider using fishing line (SPIDERWIRE ® EZ Braid, 22.7 kg tested), attached to a drive pulley with a diameter of 20.0 mm. A picture of this system can be seen in figure 12.

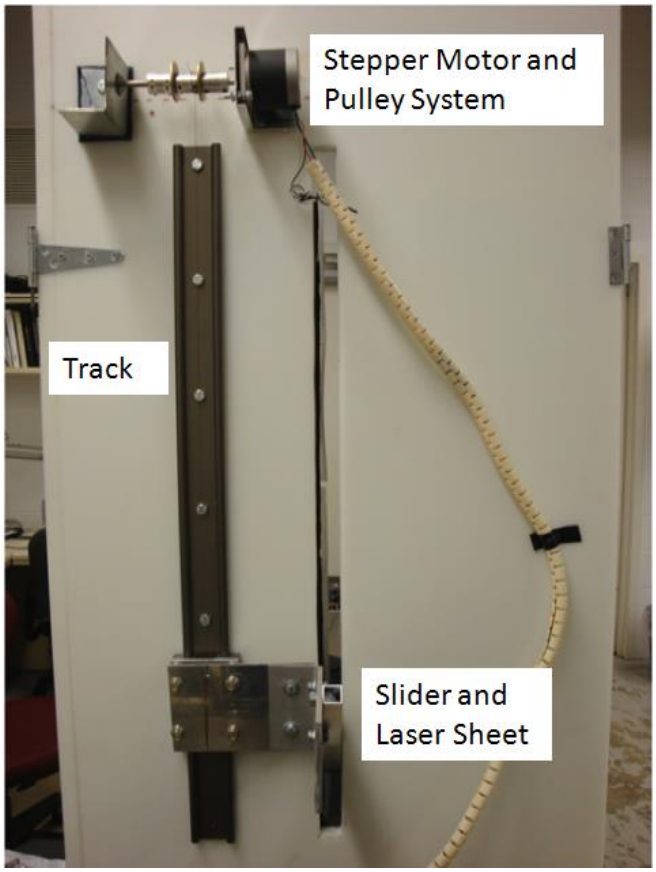

Figure 12: Photo of the mechanism that slides the laser sheet up and down along a track.

3.1.1.5 Camera System

The camera system consists of a 5 MegaPixel Unibrain® Fire-I 980b monochrome camera with an attached lens (Pentax® C60607KP). This camera was connected to a computer via a FireWire 800/800 cable running to a FireWire 800 3-Port PCI card. A picture of the UniBrain camera is shown in figure 13.

Figure 13: UniBrain 980b digital FireWire(R) monochrome camera with Pentax 6mm lens.

3.1.2 Software

The software used in this experiment performs three functions: controlling the imaging box, processing the individual image measurements, and extracting morphological features such as root angle. These functions are discussed in sections 3.1.2.1, 3.1.2.2, and 3.1.2.3 respectively. Each of the functions was controlled by a section of code written in MATLAB® (MATHWORKS, Natick, Massachusetts) version R2011b. A flowchart of this process can be found in figure 14.

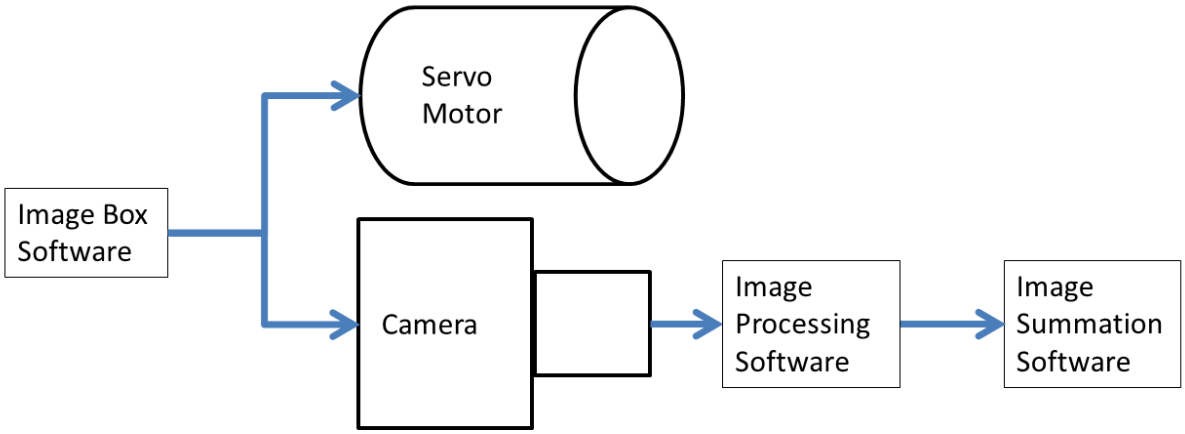

Figure 14: Overview of software functions used in the Corn Root Imaging Box with laser sheet lighting.

3.1.2.1 Imaging Box Software

The LSCRIB software controls both the camera and the servomotors in the system. The actuation of the servomotors required manufacturer's driver files and was executed as a MATLAB subroutine. The software first takes an image of the sample prior to turning on the laser. Next, the laser system is manually turned on after prompting by the program. After hitting "enter" the laser system is moved up by the servo motor increments of 6 mm by rotating the servo motor 0.9 degrees per impulse. This raising sequence is repeated a total of 20 times resulting in raising the laser system by 120 mm. Simultaneously, the imaging box control software takes an image of the projection of the laser sheet onto the corn root after each servo motor impulse.

Afterwards, the pulley system stepper motor is directed to lower the laser system 120 mm in the opposite direction, resulting in the return of the laser system cart to its starting position in preparation for the next sample. Simultaneously, the base stepper motor is sent 100 impulses, resulting in a 90 degree rotation of the sample. This process is repeated three times, resulting in four image projections of each root sample. One image produced from this software can be seen in figure 15.

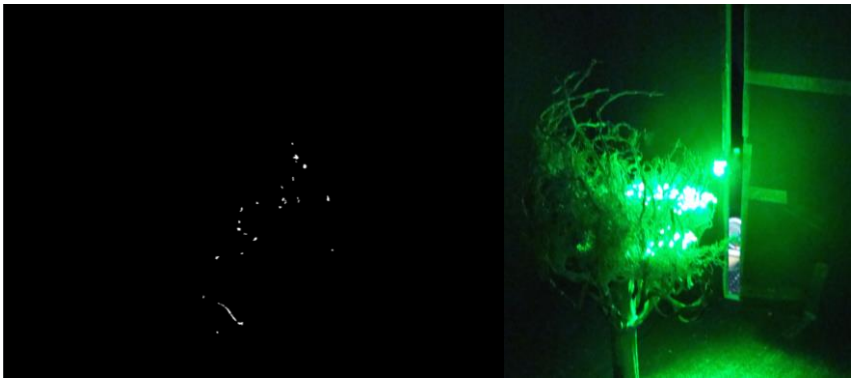

Figure 15: Left: Binary image of the interception of the laser sheet by a corn root. Right: Laser sheet illuminating a root.

The MatLab® code for this software can be found in appendix A.

3.1.2.2 Image Summation Software

The image summation software stacks each 2D image taken for one side of a sample to produce a model of that side with corresponding width and height data. This model allows for 3D visualization of the sample, both by location of pixels as well as by pixel color. One of these image summation images can be found in figure 16.

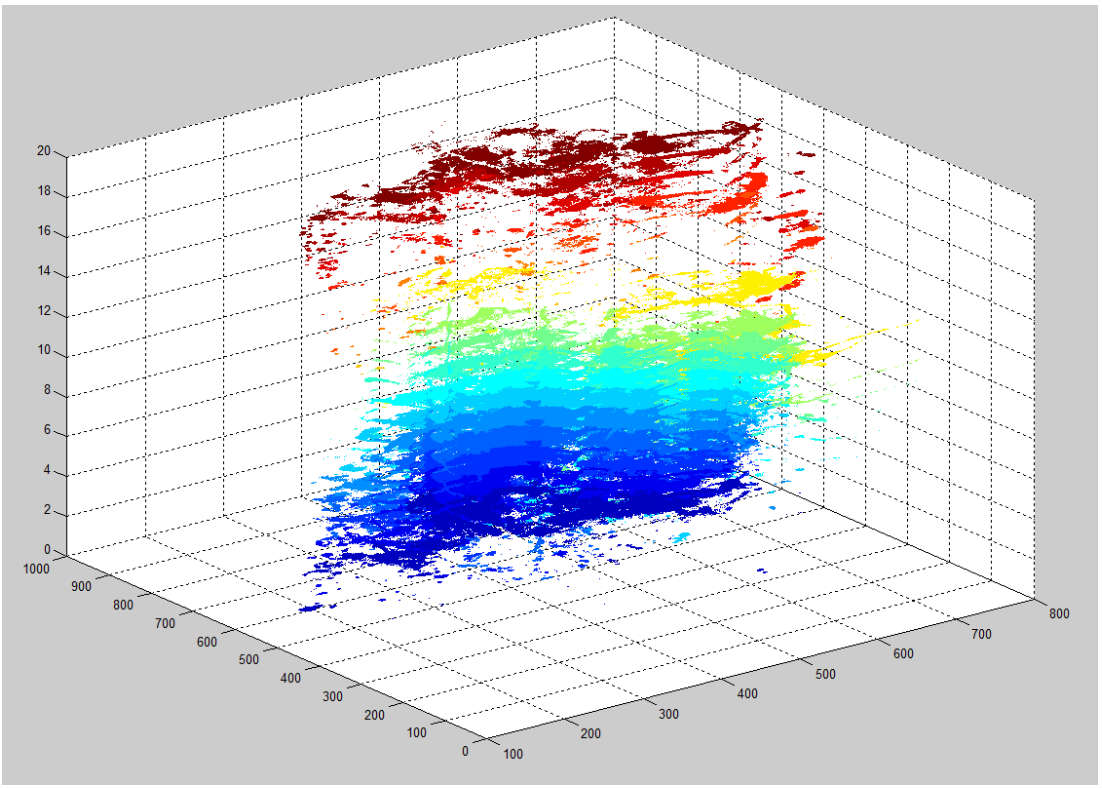

Figure 16: Summation image, where 20 images are "stacked" to give a rudimentary 3D structure of the root system.

The MatLab® code for this software used can be found in appendix B.

3.1.2.3 Image Processing Software

The image processing software determines prominent features using the technique discussed in 3.1.1 and then uses that feature to determine the height and width of the sample at that point using techniques discussed in sections 3.2.1 and 3.2.2 respectively. An unprocessed image can be seen below in figure 17 and its corresponding binary equivalent image can be seen in figure 18.

Figure 17 Original monochrome image of the laser sheet interception by a corn root. This images is later processed to yield a binary image using segmentation.

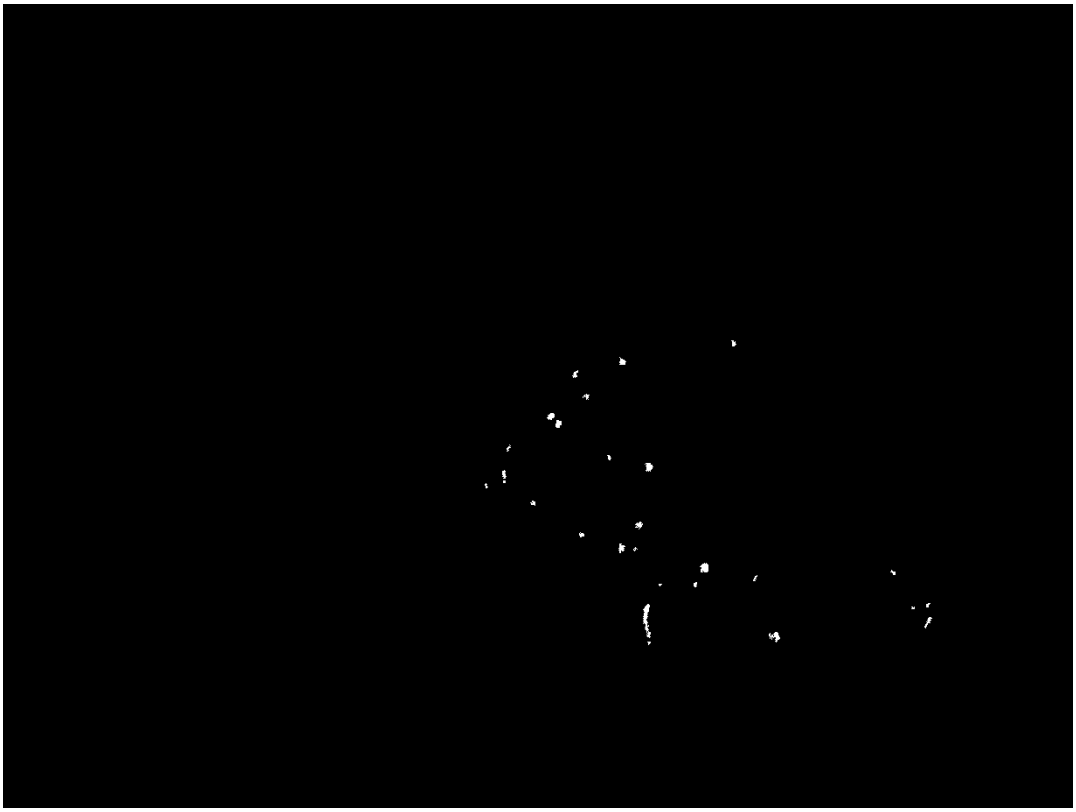

Figure 18: Binary image of laser sheet interception by a corn root after segmentation. This kind of image can be used to acquire morphological features such as the root angle.

Code for this software can be found in Appendix B.

3.1.3 Laser Sheet Measurement Apparatus Calibration

To calibrate the system, a piece of wood 177.8 mm X 38.1 mm X 876.3 mm(7 in X 1.5 in X 34.5 in) were placed within the LSCRIB leaning from the rear of the LSCRIB towards the door at a 50 degree angle from the horizontal.. The imaging box software described in Section 3.1.2.1 was then run and the resulting images were processed using the techniques described in section 3.1.2.3. This calculated the number of pixels for the laser projection at each level. By dividing the total number of illuminated pixels by the known length, conversion factors from pixels to length were determined for each level of the image. These factors can be seen in table 1.

Position Number	Conversion Factor [mm/pixels]
1	0.4023
2	0.3969
3	0.3942
4	0.3899
5	0.3848
6	0.3815
7	0.3775
8	0.3727
9	0.3681
10	0.3643
11	0.3599
12	0.3556
13	0.3514
14	0.3473
15	0.3432
16	0.3380
17	0.3342
18	0.3299
19	0.3256
20	0.3221

Table 1: Conversion Factors to convert from pixels to mm

3.2 Methodology for Measurement

This section describes the methodology used to determine width and length of the object (either a calibration object or a root). Section 3.2.1 describes the feature detection method used to conduct measurements in the image. Section 3.2.2 describes the method used to determine the length of the object. Section 3.2.3 describes the method used to determine the diameter of the object. Section 3.2.4 desdribes the method used to determine the root angle of each specimen. Section 3.2.5 describes the method used to calibrate the camera and section 3.2.6 describes the current corn root phenotyping method.

3.2.1 Feature Detection Methodology

The features of significance in each image are the bright spots caused by the laser sheet intersecting the sample. These spots correspond to the width of that section of the sample. To detect these samples, segmentation was applied. The camera output a greyscale image I. However, after viewing greyscale images output from the camera, it became clear that considerable reflectance of the laser sheet off of the sample appeared in the greyscale images. To remove these reflections, the greyscale images were converted to binary images by equation 1.

$$I_{WB} = \begin{cases} 1 \; if \; I > T_1 \\ 0 \; if \; I < T_1 \end{cases} \quad (1)$$

Where I_{WB} is the binary image converted from I, and T_1 is a threshold. T_1 for each image was computed using Otsu's method, which chooses a threshold to minimize the interclass

variance of the black and white pixels. This threshold was selected to remove reflections and noise. Additionally, it is important to remove the intersection of the laser sheet with the imaging box from the image. This is accomplished by adjusting the angle of the laser system such that the intersection of the laser sheet with the box occurs out of the view of the camera. An example of this can be seen in figure 19.

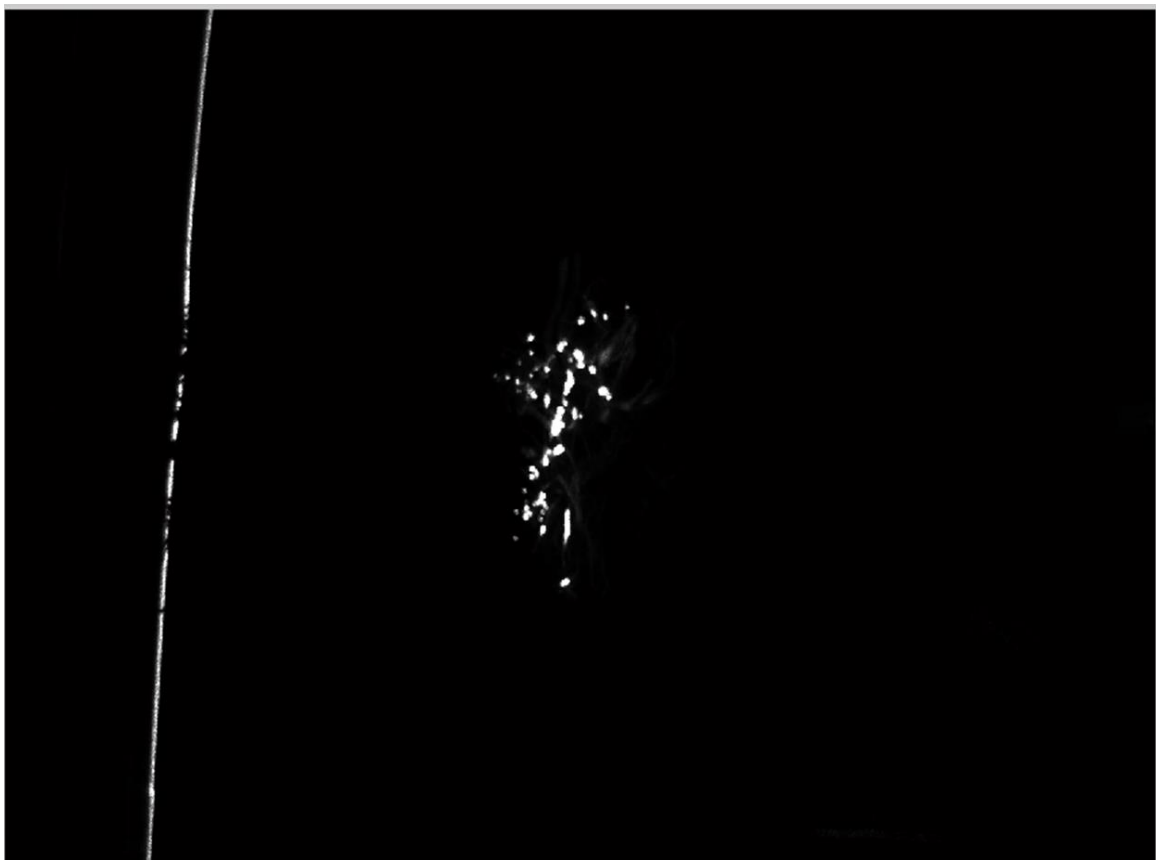

Figure 19: The original system used a laser sheet that was slanted downward at a 45 degree angle, causing the line on the left as shown in this figure. This problem was eliminated by adjusting the laser sheet to a horizontal attitude.

3.2.2 Depth Perception and Length Measurement Methodology

The distance between the camera and the object is required for length and width measurement. This distance was determined by a combination of linear interpolation and geometric analysis based on the projection of the laser sheet on the sample and the location of the laser source.

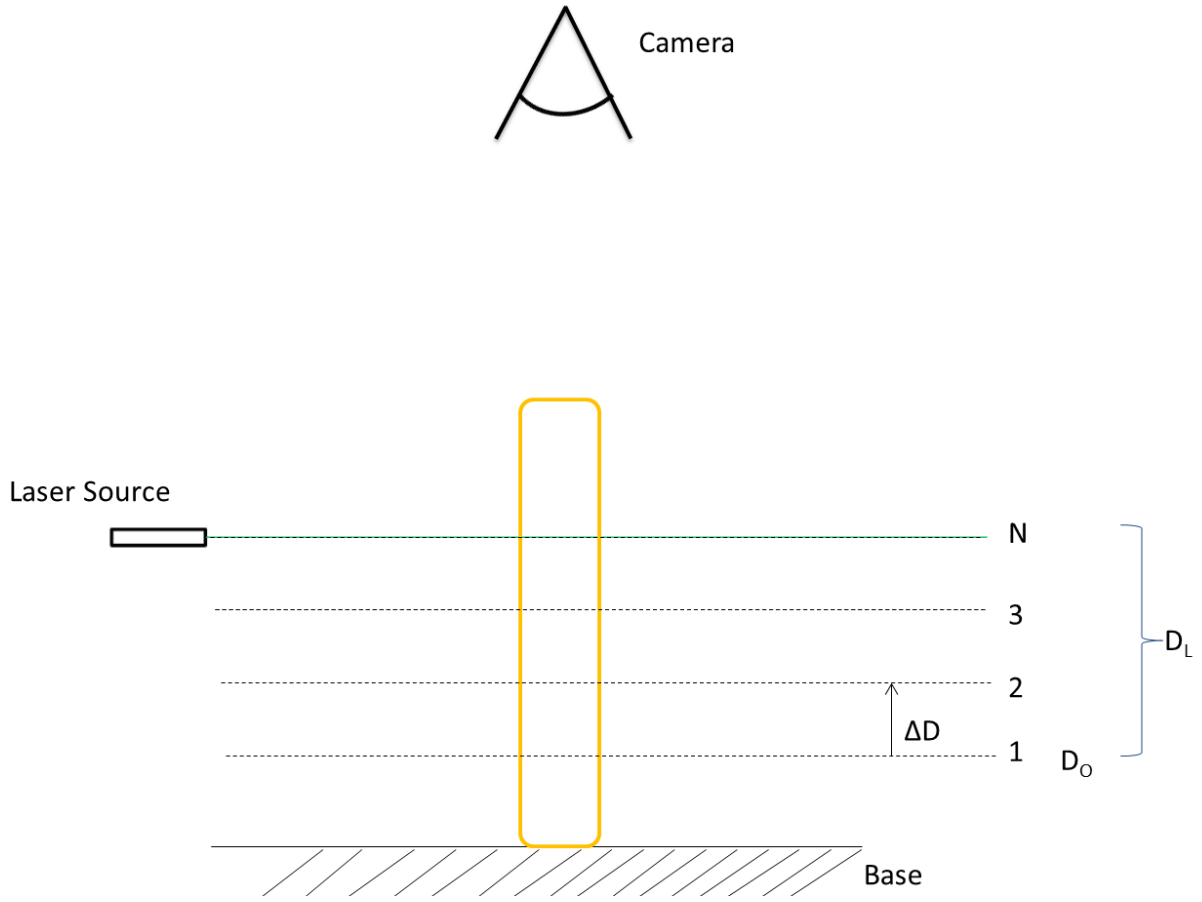

Figure 20: Model of the imaging arrangement.

Figure 20 shows a geometric representation of the rapid phenotyping apparatus. The yellow rectangle represents the sample after placement in the apparatus. D_L represents the position of the laser relative to its starting position. The beginning of each measurement cycle

begins with the Laser source positioned at D_O. After taking the initial image, the laser source is moved up in increments of ΔD to the next position (position 2) and another image is taken. This process is repeated a total of N times.

Therefore, D_L can be found at any iteration n by the following equation:

$$D_L = D_o + (n - 1) * \Delta D \quad (2)$$

3.2.3 Width Estimation Methodology

As discusses in section 3.1.3, a set of conversion factors was determined for each position of the laser sheet relative to the camera. The width of each laser illuminated portion of the sample was determined first by detecting the feature in the image. The method discussed at length in section 3.2.1 (feature detection methodology) was applied to detect the features (laser spots). The images were segmented into black and white images using the software described in section 3.1.2.3. Then, a bounding box was drawn around the remaining figures as shown in Figure 21.

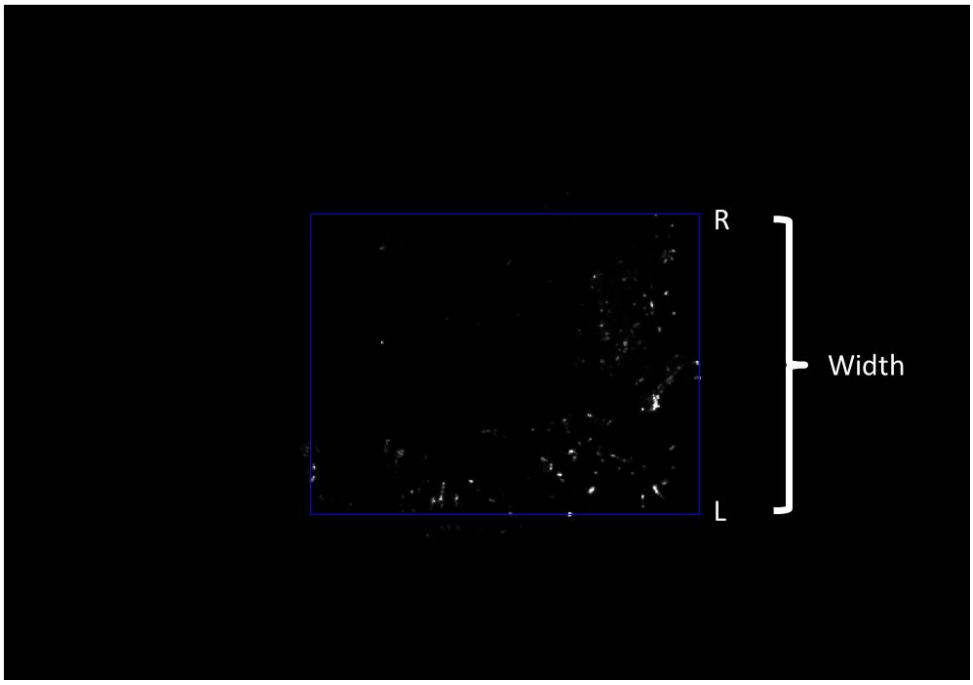

Figure 21: Laser sheet interception image, and bounding box showing the outer dimensions of the intercepted root structure.

The width for each sample in pixels was found by subtracting the vertical coordinate of the lower coordinate of the bounding box L from the upper coordinate R as shown by equation 3.

$$\mathbf{Width\ [pixels]} = \mathbf{R} - \mathbf{L} \tag{3}$$

The sample width in pixels was converted into mm by multiplying each pixel width by its corresponding conversion factor as shown by equation 4:

$$\text{Width [mm]} = \text{Width [pixels]} * \frac{\text{mm}}{\text{pixels}} \tag{4}$$

3.2.4 Root Angle Estimation Methodology

The root angle estimation methodology relies on the assumption that a corn root can be approximated by a cylindrical section (stalk) and a conical root mass. The width of each image was found using the methodology in section 3.2.3. The vertical separation between each image is 6mm.

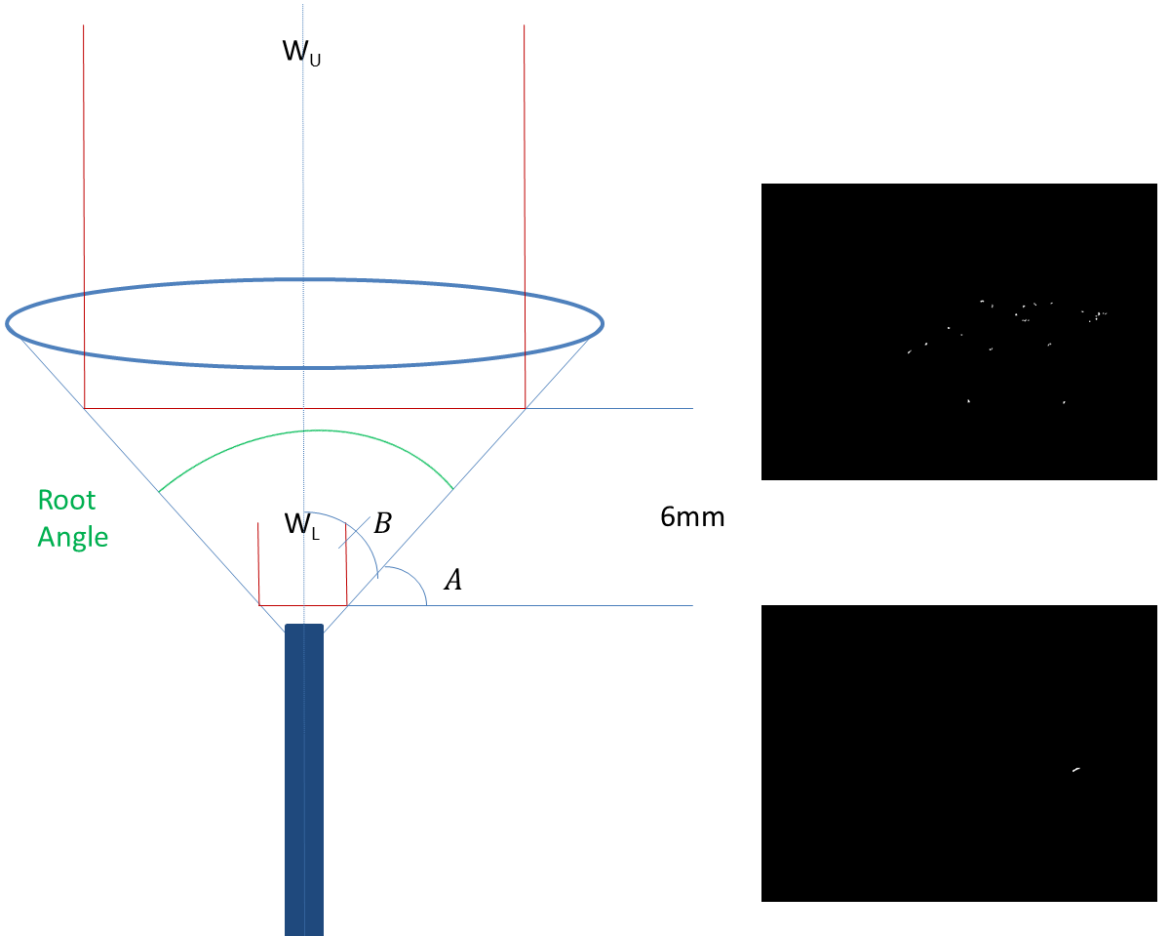

Figure 22: Simple abstraction of a corn root (upside down), allowing for measurement of the root angle based on laser sheet interception. The figures on the right show that images acquired at two levels, stalk (bottom) and root mass (top).

Figure 22 shows a geometric representation of the corn root sample, based on a cylinder/cone model. The blue rectangle represents the stalk and the cone represents the root mass. Widths W_L and W_U represent the lower and upper measured widths. These two width measurements are separated by 6mm vertically. Figure 23 shows a simple extraction of the width data gathered from the LSCRIB. Angle G is the rate of the

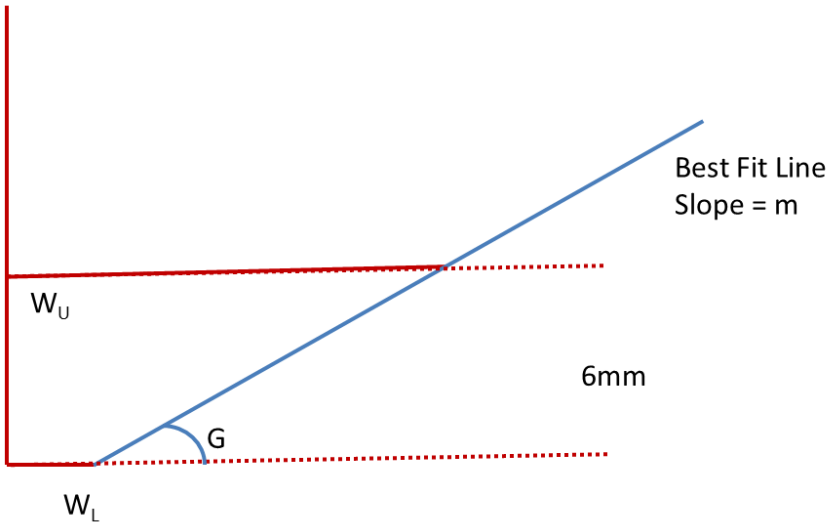

Figure 23 Simple Extraction of the data gathered from the LSCRIB

By trigonometry, it is apparent that the angle G can be found by the slope of the best fit line by:

$$G = \arctan(m) \tag{5}$$

The root is assumed to be conical and symmetric. Therefore, by geometric interpolation, it is apparent that

$$G = A/2 \tag{6}$$

and

$$\mathbf{B = 90° - A = 90° - 2G = 90° - 2 * \arctan(m)} \quad (7)$$

Therefore, the root angle can be found by equation 8:

$$\text{Root Angle} = 2B = 2(90° - 2\arctan(m)) \quad (8)$$

3.2.5 Camera Calibration Methodology

To reconstruct three-dimensional information optically, calibration of the cameras used is required (Tsai, 1987). This process determines the intrinsic and extrinsic parameters of the camera. The intrinsic parameters (effective focal length f, scale factor s_u, and the image center coordinates) determine the camera's geometric and optical characteristics. Calibration was conducted according to Heikkilä, (1997) using 25 checker board images at various angles. A mosaic of the images used for this calibration can be seen in figure 24.

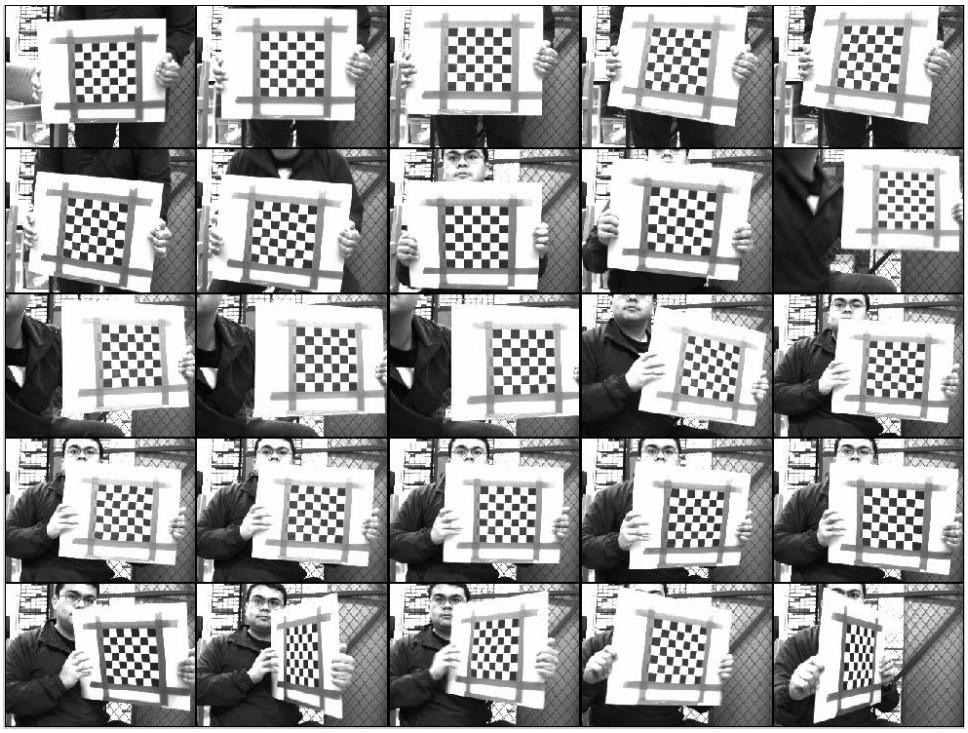

Figure 24: Image set used for calibration of the camera.

3.2.6 Current Corn Root Phenotyping Method

To determine the effectiveness of the new apparatus, a phenotyping method currently in use by the UIUC phenotyping lab was used on the same samples of corn roots that were measured using the new rapid phenotyping techniques discussed in section 3.1. The current technique was developed at the UIUC (Grift et al., 2011). It uses a system of two monochrome industrial cameras in conjunction with controlled lighting to produce images of corn roots. This system can be seen in figure 25.

Figure 25: Photo of the current corn root imaging box (CRIB) that features diffuse lighting and an automated system that rotates the roots.

After acquisition, the images were analyzed using a proprietary image analysis program to measure root angle and root complexity. One such image can be seen in figure 26.

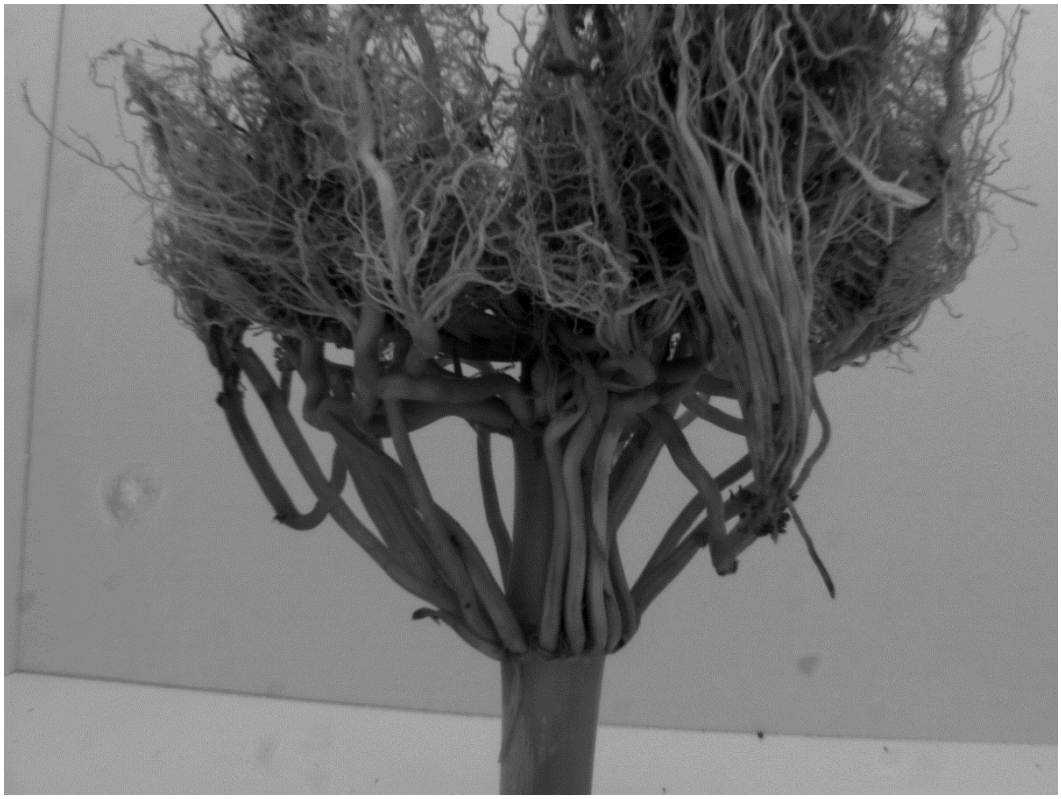

Figure 26 Image of a sample taken on the CRIB

3.3 Sample Preparation

Experiments were run on both corn tassels and roots. Both sample sets were provided by Dr. Martin Bohn and were removed from a field by the author at the UIUC South farms. Section 3.3.1 describes the selection and preparation of the corn tassel samples. Section 3.3.2 describes the selection and preparation of the corn root samples.

3.3.1 Corn Tassel Samples

Corn Tassel samples were taken from an ongoing project within the CS department. Twenty samples were taken from the field. An example of one of these samples can be seen in figure 27.

Figure 27: Example of a corn tassel that could potentially be analyzed using the laser interception method.

One of the tassel samples was then prepared for the experiment by removing the tassels from the standing corn plants, removing the leaves, trimming the samples to 450 mm length, and attaching the tassels to the rod in the base of the apparatus using electoral tape as shown in figure 28.

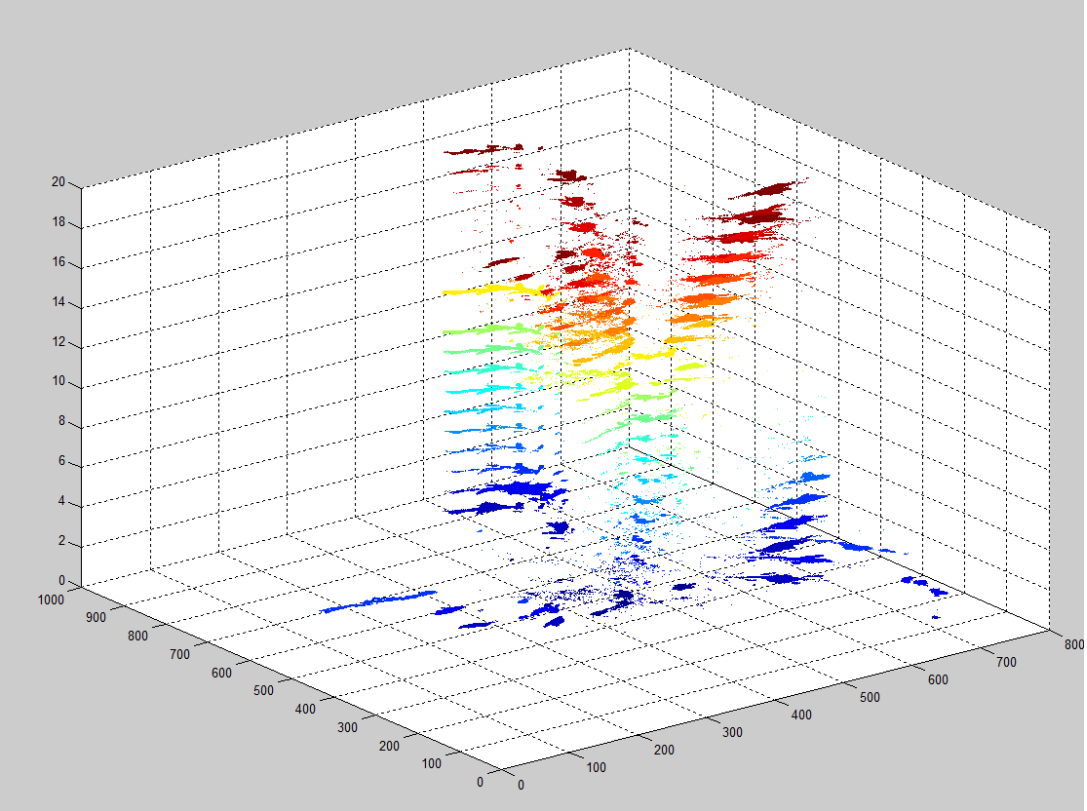

Figure 28: A 3D image of a corn tassle sample made from 2D images produced on the LSCRIB

3.3.2 Corn Root Samples

Corn root sample were taken from an ongoing project within the CS department. After harvesting, the samples were cleaned through a combination of soaking and vigorous shaking in water buckets as shown in figure 29.

Figure 29: Corn roots being soaked in buckets to prepare for imaging.

This was followed by further cleaning with water hoses as shown in figure 30.

Figure 30: Cleaning of corn roots was done by soaking and washing.

Then the samples were trimmed to 300 mm in length and any non-root material was removed manually. An example of a root containing non-root material after soaking and washing can be seen in figure 31.

Figure 31: Example of a corn root that has non-corn matter. Clay rich soils, such as found in Central Illinois, cause ample non-corn matter to be firmly attached to the root.

A hole was then made into the stalk with a screwdriver as shown in figure 32.

Figure 32: Corn roots were mounted in the imaging system by putting them on a spike. This was done by poking a 1/4 inch hole in the stem of the roots.

CHAPTER 4

EXPERIMENTAL DESIGN

In this chapter, the assumptions and experiment of various stages of this experiment are introduced. Section 4.1 discusses the camera calibration results. Section 4.2 discusses the implementation of the apparatus discussed in section 3.2. Section 4.3 discusses the measurement results after applying the initial image processing software. Section 4.4 discusses the results after applying the image summation software.

4.1 Camera Calibration Results

The intrinsic parameters of the camera are shown in table 2.

Focal Length (pixel)	[1816.46 1817.69]
Principal Point (pixel)	[669.76 376.30]
Skew Angle (degree)	90
Distortion Coefficients	[-0.10640 -1.49936 0.00144 0.00650 0.00000]

Table 2: Intrinsic parameters of the camera system.

4.2 Implementation of the LSCRIB

The rapid phenotyping apparatus based on the LSCRIB discussed at in section 3.2 was implemented into the instrumentation and robotics laboratory in the ABE department at the University of Illinois. A picture of this setup can be found in figure 33.

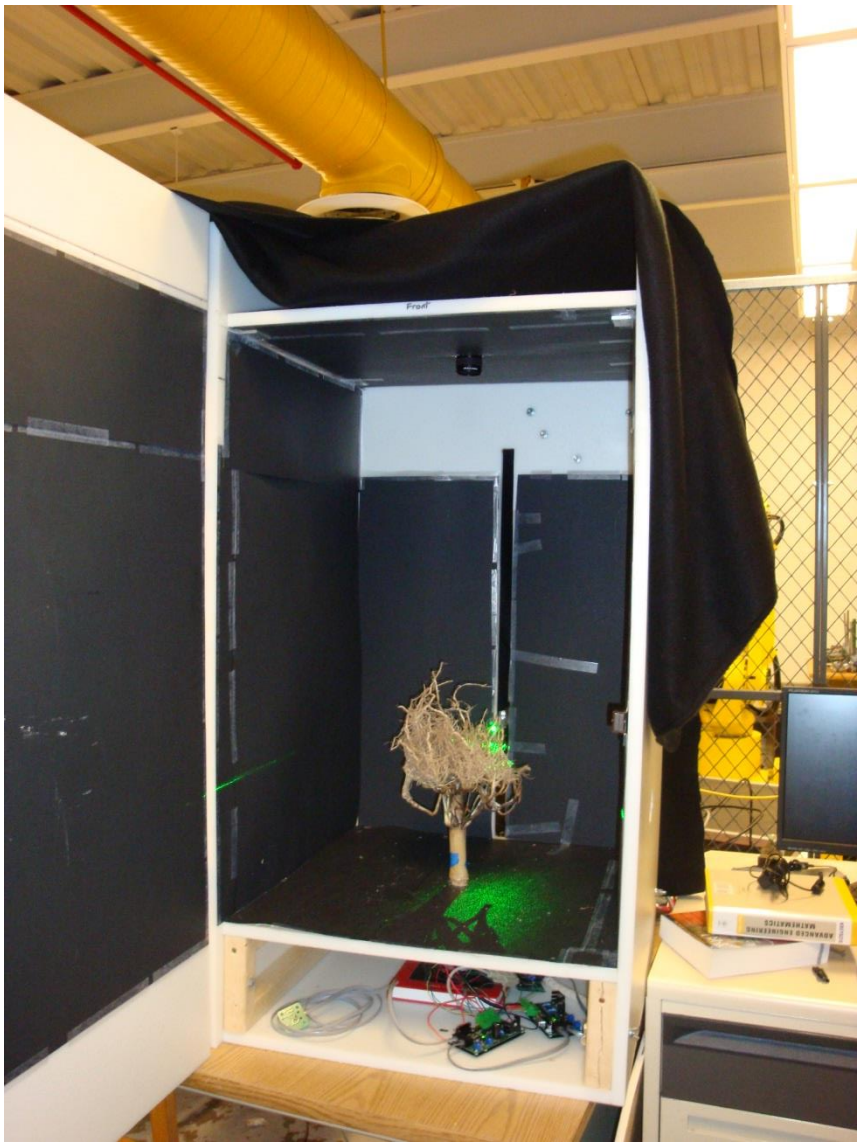

Figure 33: Photo of the complete Laser Sheet Corn Root Imaging Box (LSCRIB).

Samples were prepared as discussed in section 3.3, and placed inside the CRIB. The apparatus was operated and the sample images recorded. The samples were subsequently measured using manual phenotyping process and the measurements recorded.

4.3 Initial Image Processing

After examining the images produced by the apparatus, it became apparent that there were two primary sources of error found in the images: reflections of the laser sheet off of the sample and laser sheet projections into the background. A raw image showing these errors can be found in figure 34.

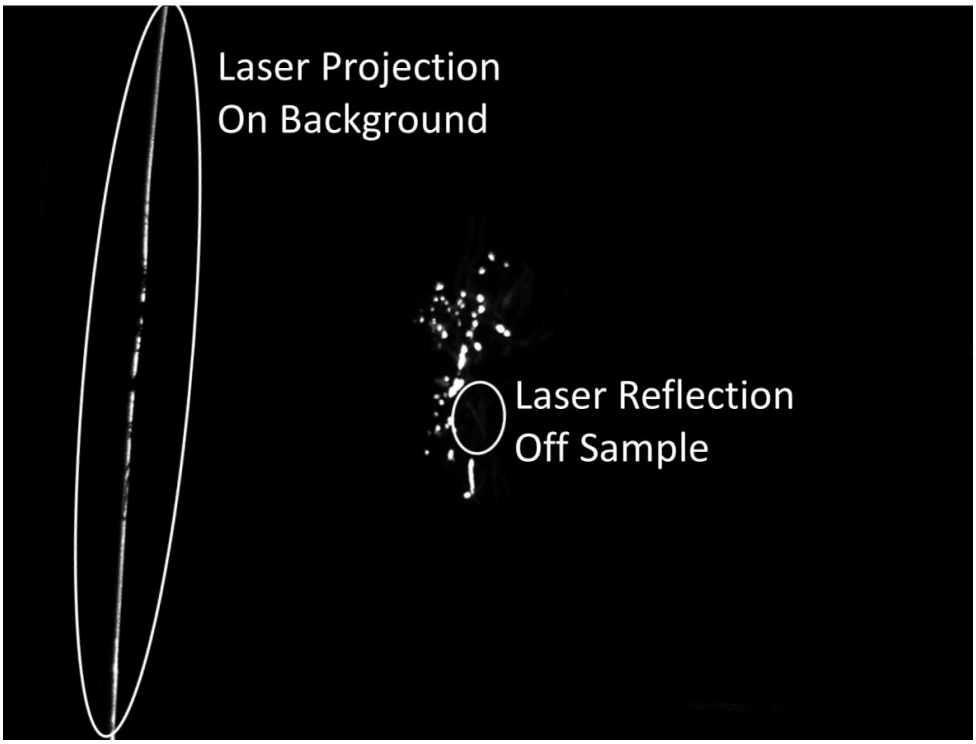

Figure 34: This image shows a laser line projected onto the background (due to original 45 degree slanted laser sheet) as well as reflections of the laser sheet onto other root parts.

To minimize the effect of the laser reflection off of the sample, each image taken by the camera was converted from a monochrome image into a binary image. By setting the threshold for the binary image such that the intensity of the reflected light was not high enough to be counted as a “white” area, the effect of the laser reflection was reduced as shown by figure 35.

Figure 35: Reflected laser light areas were removed by segmentation of the original image.

In order to remove the laser projection from the image, the angle of the laser sheet was adjusted from 45 degrees to 0 degrees. One of the resulting images can be seen below in figure 36.

Figure 36: Image of laser sheet interruption without the line in the background by setting the laser angel from 45 to 0 degrees.

4.4 Effects and Results After Image Summation

The images taken for each sample were summed, resulting in a composite image. One of these images can be found in figure 37.

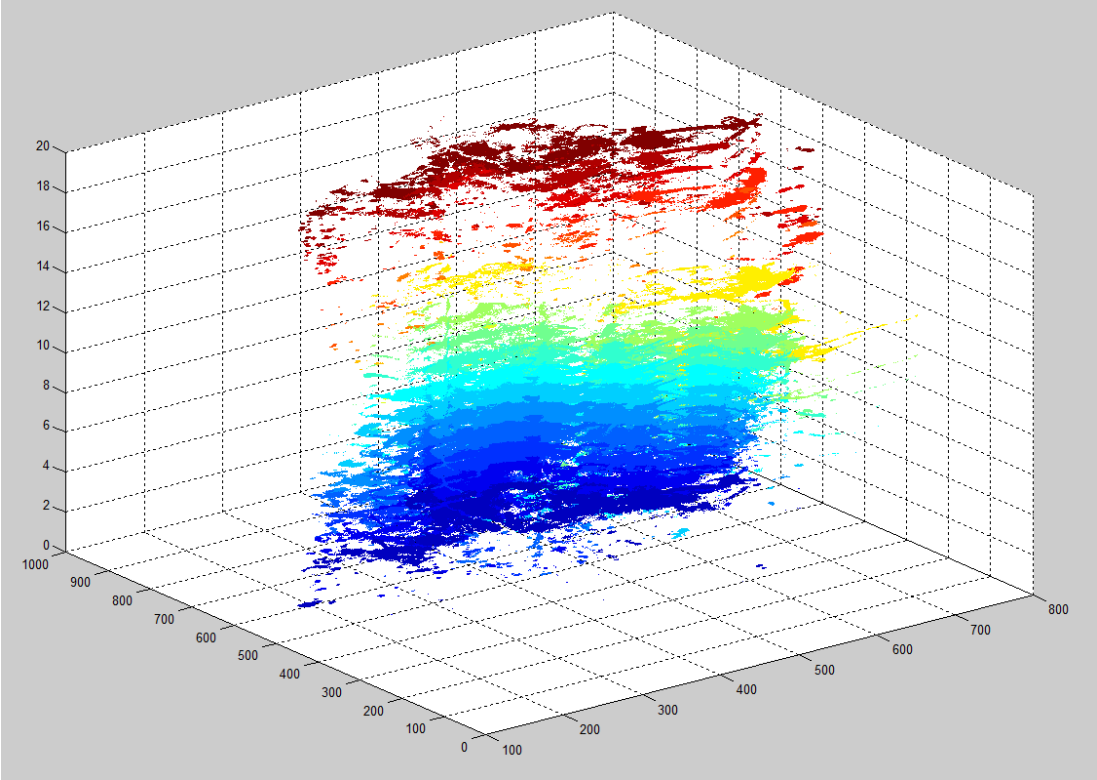

Figure 37 Result of image summation, where the root structure can be vaguely recognized. This image can be improved by adding more images at a high vertical movement resolution of the laser sheet.

4.5 Results and Discussion

Section 4.5.1 discusses the results accomplished during this thesis. Section 4.5.2 discusses the primary sources of error encountered during this experiment.

4.5.1 Results Accomplished During this Thesis

Section 4.5.1.1 compares the results acquired by the LSCRIB and compares those results to those acquired by the CRIB. Section 4.5.1.2 describes the results acquired by computer tomography. Section 4.5.1.3 describes the results acquired by magnetic resonance imaging.

4.5.1.1 LSCRIB Results Evaluated Against CRIB Results

20 samples of corn roots were harvested and prepared according to section 3.3.2. These samples were run on both the LSCRIB and the CRIB machines. The CRIB produced results of the sort shown in figure 38.

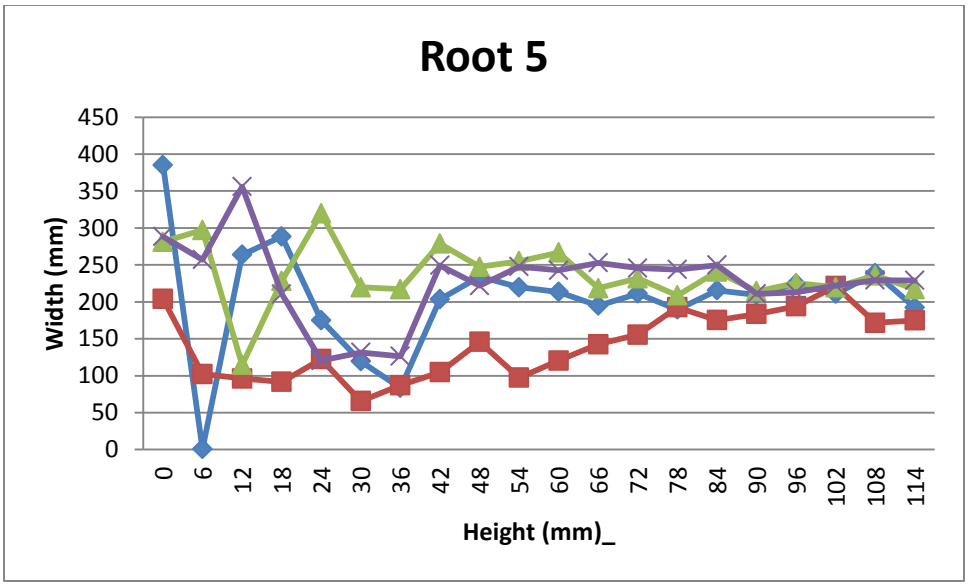

Figure 38: Root Height vs Width for all data generated on one sample using the LSCRIB. Each color represents a separate scan for the root.

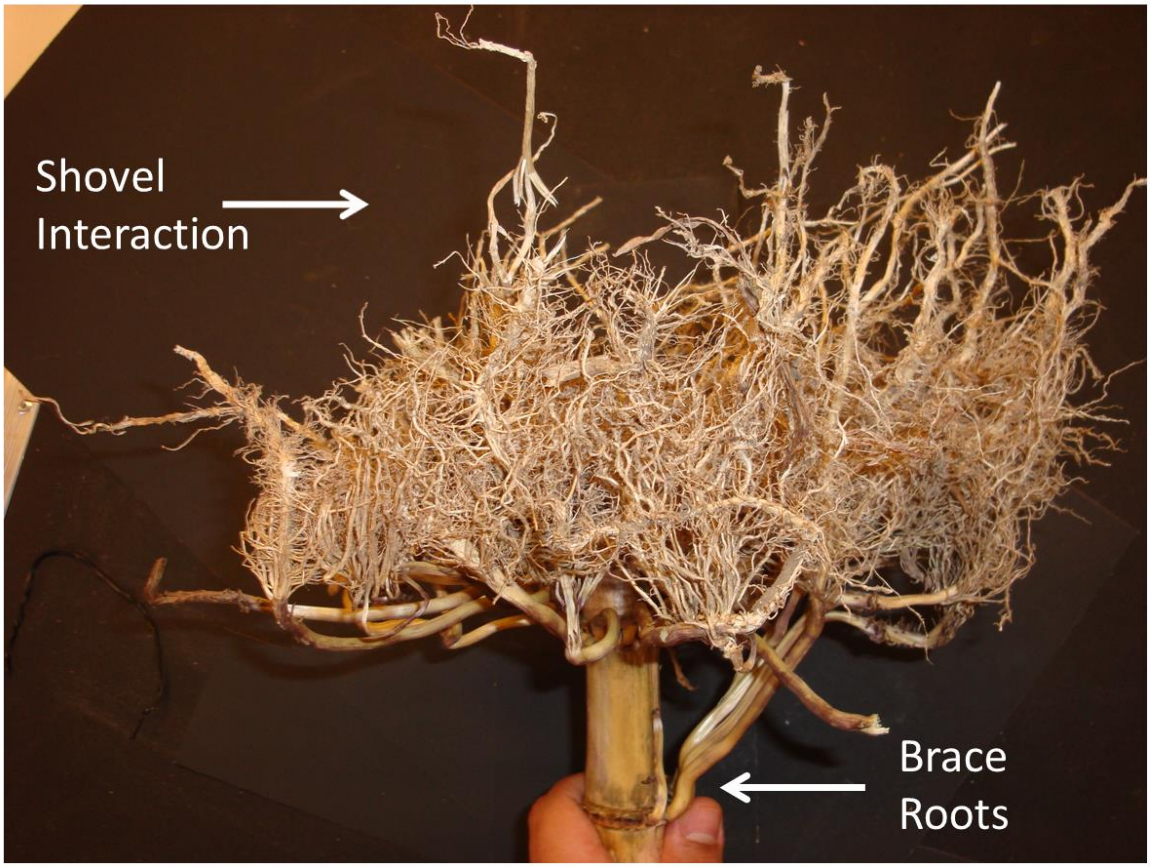

Figure 39 Example of Brace Root Structure and Shovel Interaction encountered during this experiment.

There are two main sources of irregularity in the images: the bottom (due to brace roots), and the top (due to the shovel cutting the root at an angle). These can be seen in figure 39. In order to minimize these known sources of error the first five and the last five scans from the data were removed. Therefore, only the central 10 scans are used for determining the root angle. A best fit line is drawn through the data points. This can be seen in figure 40.

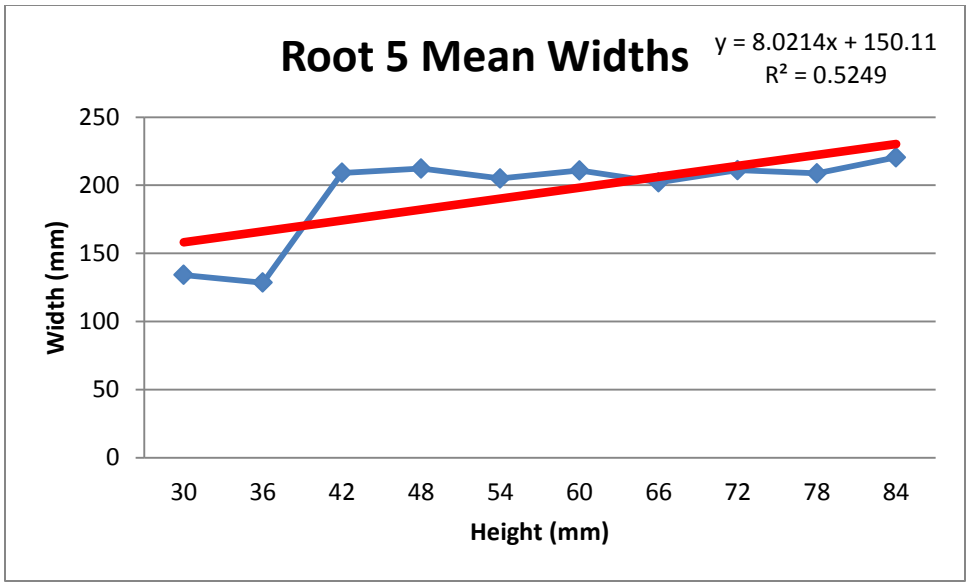

Figure 40 Root height vs width after initial and final datapoints are removed.

The slopes of the best fit line were then used determine the root angle for each sample according to the methodology described in section 3.2.4. The same samples were examined using the CRIB apparatus in section 3.2.5. The results of both sections can be seen in the table 3.

Sample	CRIB Root Angle (degrees)	LSCRIB Root Angle (degrees)
1	134.3	368.5
2	127.0	234.2
3	194.5	185.7
4	115.0	312.1
5	121.8	-151.6
6	140.5	-104.7
7	112.3	-100.5
8	110.0	517.4
9	125.5	512.4
10	114.8	525.3
11	123.8	511.2
12	115.0	521.9
13	127.8	1.7
14	148.8	496.7
15	156.5	508.1
16	120.5	525.4
17	109.3	521.3
18	86.3	526.4
19	111.5	511.0
20	151.5	467.6

Table 3: Data on Corn Root angles from the CRIB and the LSCRIB

In order to allow better visualization of the LSCRIB root angles, all root angles were converted to angles between 0 degrees and 360 degrees by adding or subtracting 360 degrees. The results can be seen in table 4.

Sample	CRIB Root Angle (degrees)	LSCRIB Root Angle Converted (degrees)	Percentage Difference
1	134.3	8.5	93.7
2	127.0	234.2	84.4
3	194.5	185.7	4.5
4	115.0	312.1	171.4
5	121.8	208.4	71.2
6	140.5	255.3	81.7
7	112.3	259.5	131.2
8	110.0	157.4	43.1
9	125.5	152.4	21.4
10	114.8	165.3	44.0
11	123.8	151.2	22.2
12	115.0	161.9	40.8
13	127.8	1.7	98.7
14	148.8	136.7	8.1
15	156.5	148.1	5.4
16	120.5	165.4	37.3
17	109.3	161.3	47.6
18	86.3	166.4	92.9
19	111.5	151.0	35.4
20	151.5	107.6	29.0

Table 4: Data on Corn Root angles from the CRIB and converted Corn Root angles from the LSCRIB

4.5.1.1 Computer Tomography for Phenotyping.

A corn root sample was placed into a SIEMENS Inveon PET•SPECT•CT scanner and a CT scan was conducted on the sample. Afterwards, the individual x-ray slices were combined into a 3D model. This can be seen in figure 41.

Figure 41: CT scan of a corn root. Although these images have an extreme resolution (40 micrometer), the acquisition and data analysis required 80 minutes, and the cost was around $120.

The images produced using CT are of extremely high resolution (40 microns). The system is capable of producing images of up to 14 micron resolution. This is much higher resolution than is capable with conventional optics. Additionally, CT systems produce data about

internal structure and are unaffected by occlusion. There is potential to use the data generated from CT images to calibrate other phenotyping systems. CT can also be applied to systems containing soil, potentially reducing the time needed to prepare samples.

The major issues with using CT for phenotyping are low throughput and high capital cost. Each 3D model takes up to 80 minutes to process. This is primarily due to the time needed to convert the 2D images into a 3D model. Also, CT machines are orders of magnitude more expensive than either the CRIB or the LSCRIB, making investment in such machines difficult to justify for many plant breeders.

4.5.1.2 Magnetic Resonance Imaging for Phenotyping

A corn root sample was placed into a 600 MHz Varian MR system consisting of a 14.1T wide bore magnet. 20 cross sectional images and 10 lateral images were taken. An example of these images can be seen in figure 42.

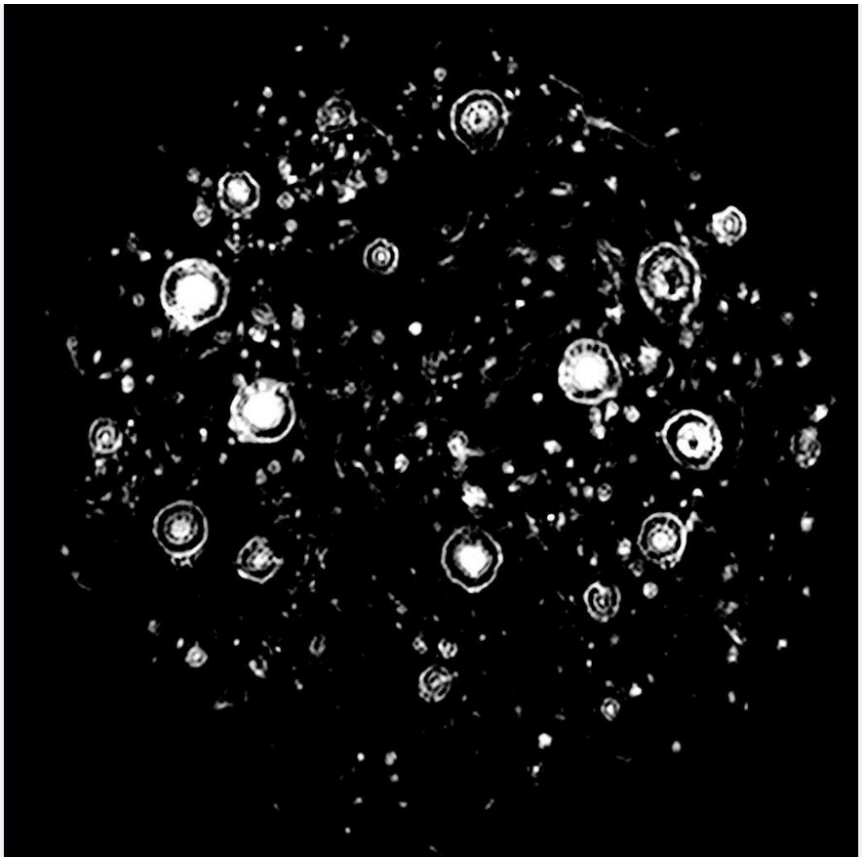

Figure 42: The MRI technique can yield very high resolution cross sectional imagery, but as in the case of CT, the required acquisition time and cost are high.

The images produced using MRI are of extremely high resolution. The system is capable of producing images of up to 4 micron resolution. This is much higher resolution than is capable with conventional optics. Additionally, like CT systems, MRI systems produce data about internal structure and are unaffected by occlusion. This also leads to potentially using data generated by MRI images to calibrate other phenotyping techniques. MRI can also be applied to systems containing soil, potentially reducing the time needed to prepare samples. MRI can also be used to determine the chemistry at points determined within the image.

Like CT, the major issues with using MRI for phenotyping are low throughput and high capital cost. Each 3D model takes up to 120 minutes to process. This is primarily due to the time

needed to convert the 2D images into a 3D model. MRI machines are orders of magnitude more expensive than either the CRIB or the LSCRIB, making investment in such machines difficult to justify for many plant breeders.

4.5.2 Primary Sources of Error

There are many factors encountered in this experiment that can contribute to measurement error. These include reflections from the laser sheet, excess light entering the imaging chamber, and improperly drilled holes in the samples. However, the primary sources of error encountered in this experiment come from four sources: repeatability errors in the positioning of the laser system, thick illuminated sections of the sample, pixel measurement error, and shadowing of portions of the sample. These are discussed in sections 4.5.2.1, 4.5.2.2, and section 4.5.2.3 respectively.

4.5.2.1 Laser Distance Repeatability Error

As described in sections 3.2.2 and 3.2.3, the measurement technique relies on the distance between the laser system and the camera to measure both distance and width. This distance is not fixed; it changes for each image of a sample as the laser sheet is moved to illuminate a different section. Error due to this is significant as the repeatability of the pulley system is limited owing to slippage in the pulley system, irregular wrapping of the fishing line around the pulley, and irregular friction between the slider and the rail system along its path. To determine this extent of this error, a test was conducted on the repeatability of the laser distance positioning system: The

positioning cart was first raised 10 steps from its bottom position. The location of the cart relative to the apparatus was marked with tape on both the cart and the board. Then, the cart was raised 10 steps and then immediately lowered 10 steps and the difference between the initial position and the final position was recorded. This process was repeated 20 times. The mean difference in position from the previous run is 0.12 mm. Changing the laser positioning system to a more repeatable system should decrease the effects of this error source. This is particularly important when utilizing such a system in a crop science laboratory due to the presence of large quantities of particulate matter. This particulate matter will stick to the lubrication on the open rail system, increasing the coefficient of friction the stepper motor must overcome when raising the laser positioning system.

4.5.2.2 Laser Sheet Thickness

An additional significant source of error encountered in this project is the thickness of illuminated sections of the sample, caused by the laser sheet thickness of approximate 3 mm. In irregular shapes (such as encountered in corn roots), this causes significant error in width measurements. The largest width measured is recorded for each segment leading to a bias towards large width measurements. Reducing the effects of this phenomenon can be accomplished by reducing the size of the illuminated section of the sample – essentially illuminating smaller slices of the sample per image. An image showing the illuminated section can be seen in figure 43 below.

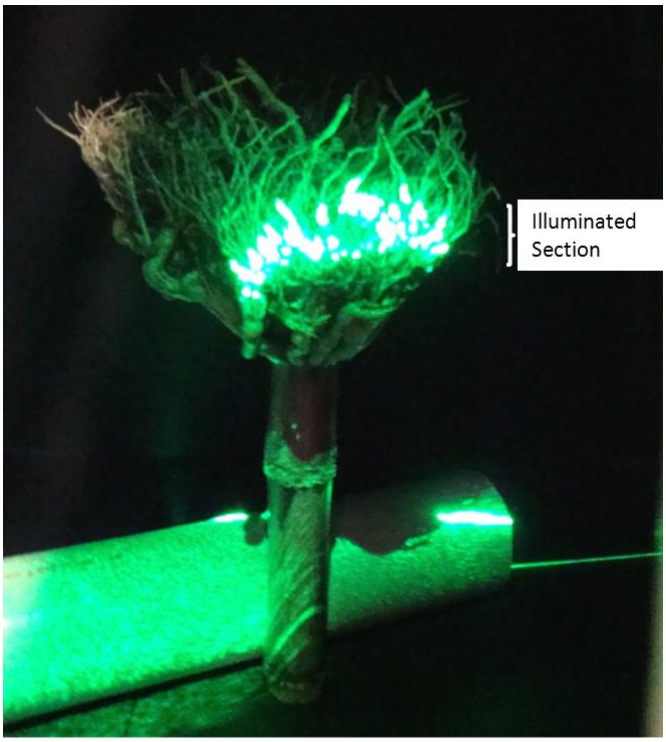

Figure 43: The thickness of the laser sheet limits the resolution with which small root features can be detected in the images.

4.5.2.3 Occlusion

Occlusion of the sample is a major source of measurement error. As the laser source illuminates the sample, the illuminated area casts a shadow on areas immediately behind it. This limits the detail that can be observed (and measured) by the camera system to that which can be illuminated by the laser system. Shadowing also limits the areas of the sample that can be measured. If an area of the sample has a thicker area above it (such as the stalk of an inverted corn root sample), it will be missed entirely by this measurement technique. This can be seen in figure 44 as the laser sheet clearly strikes the corn stalk (as shown by the hole in the laser sheet) but the intersection of the sheet remains occluded due to the root structure above.

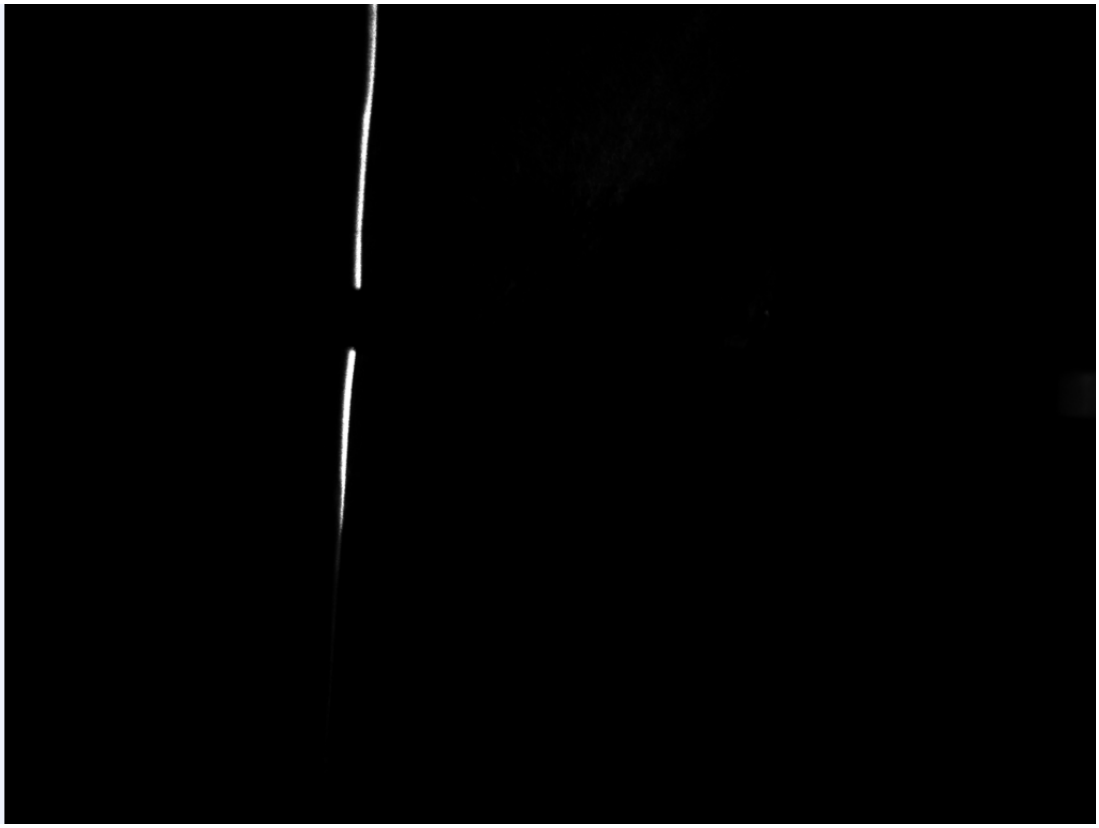

Figure 44: Example of shadowing where the root stalks casts a large shadow onto the background.

CHAPTER 5

CONCLUSIONS AND RECOMMENDATIONS FOR FUTURE WORK

Section 5.1 of this chapter summarizes the achievement of this study and addresses the research objectives stated in section 1.2. Section 5.2 describes insights and identifies inefficiencies of this study.

5.1 Summary

Several corn roots were obtained and prepared for experimental use. These roots enabled proof-of-concept experiments in the laboratory. A custom laser root scanner was built for this research. Software written in MATLAB® was also developed to both control the laser root scanner and to process the images.

Code was developed to control the camera and laser positioning system of the apparatus. For positioning, the code controlled a servomotor which controlled the laser position by rotating a pulley system that raised and lowered a cart on a rail. This positioning system was tested and found to be precise. The same code also rotated the sample, allowing for multiple sides to be examined.

The images produced by the camera were further refined by converting them to binary images in order to reduce the effects of reflections and unwanted light sources. The images were then compared to images of samples of known diameter, allowing for measurement of the

diameter of the root structure at the points intersecting with the laser sheet. Additionally, the angle of the root perimeter from the root stem was found for each laser sheet intersection, allowing for root angle measurement. On average, the scanning of prepared root samples required 5 minutes from placement of the sample into the imaging chamber to final image. This is comparable to the time needed to analyze roots using the CRIB. Also, the LSCRIB requires minimal training to operate, reducing training costs in a production environment. A program was also developed to allow 3D visualization of the root structure by stacking the images taken during the experiment.

Additional methods for phenotyping were also explored. Corn root samples were run both a CT and an MRI machine and the resulting images were examined, proving the technical potential for both systems in phenotyping. The economic feasibility of utilizing both measurement techniques for phenotyping was also examined. In conclusion, this study successfully validated a three-dimensional corn root scanner and proved the concept using a custom built apparatus. Additionally, two different high definition imaging techniques were also validated for use in phenotyping corn roots.

5.2 Recommendations for Future Work

This thesis has demonstrated the concept of 3D visualization using a mobile laser sheet and a static camera; various issues remain unsolved and need to be addressed in the future. Section 5.2.1 describes methods to optimize component selection for future versions of the machine. Section 5.2.2 describes other measurement opportunities to which this technique can be applied.

5.2.1 Recommended Component Selection

While selecting components for future laser measurement systems, mitigation of error is an important criterion to consider. To mitigate the primary sources of error described in section 4.5.2 (location repeatability of the laser system, thick illuminated sections of the sample, pixel measurement system, and shadowing of portions of the sample), careful selection of key components is imperative.

To mitigate the error produced by moving the laser system for each measurement, selection of a mechanism to move the laser system in a highly repeatable fashion is needed. One method to accomplish this is to utilize a belt driven linear motion system. One such system that would accomplish this is the Techno Inc. Linear Motion ZF1 Belt Drive Slide Model number HL3105MP070S. Per the advertised product literature, the system is repeatable to within ±0.01 mm and accurate to ± 0.2 mm/300mm. A picture of such Techno Inc. Linear Motion ZF1 system can be found in figure 45. Additionally, a robotic arm could be used for the same purpose, allowing for the laser system to be maneuvered around the sample so that other sides of the sample can be illuminated and measured.

Figure 45: Techno Inc. Linear Motion ZF1 system. This linear motion system has a high resolution and precision, and can be used to improve the image acquisition process in the future. From: http://www.techno-isel.com/tic/Catdas/PDF/ZF1.pdf. Accessed 11/27/2013/

To mitigate issues associated with the thick sections of sample illuminated by the laser sheet, a Fresnel lens that produces a thinner laser sheet than the one used should be selected. This would essentially allow the laser system to illuminate thinner slices of the sample, decreasing the effect of irregular sample segments in overestimating sample width.

The use of a higher resolution camera or a camera lens equipped with a zoom feature would reduce the effects of pixel estimation error in measurement error by increasing the number of pixels per unit area measured.

In order to mitigate the effects of shadowing on the several issues must be addressed. Firstly, the effects of shadowing may be mitigated by imaging additional sides of the sample. This can be accomplished by mounting the laser sheet onto a platform that can move around the sample (such as a robotic arm) or by rotating the sample. An additional method to reduce the effects of shadowing could be accomplished through the use of other imaging techniques on roots. For instance, the use of x-rays in a 3D scanner (such as a CT scanner) would eliminate much of the effects of shadowing as the x-rays penetrate outlying structure, allowing imaging of previously hidden root structure. This would allow analyzing of extremely complex root structures, such as miscanthus giganteus (figure 46).

Figure 46: Root mass of Miscanthus giganteus, with a highly intricate structure.

Additionally, samples must be free from material that causes shadowing. This is especially common for root samples as clumps of soil in the root samples occlude large segments

of the root structure, limiting the usefulness of root complexity measurements. This is accomplished via cleaning the samples manually with a dunk tank followed by pressurized water. Automating the root cleaning procedure would reduce the occurrence of non-root material in the samples, particularly when inexperienced technicians are cleaning the root samples. This would also have the effect of increasing throughput in the most labor intensive step in the root scanning procedure.

Experience with the apparatus described above has shown that further refinement to the apparatus would be beneficial. For example, selecting a lighter weight, non-transparent material for constructing the box would be beneficial. This would decrease weight and eliminate the need to line the interior of the box with black cardboard – increasing the durability of the apparatus. A lighter power source for the laser provides another opportunity to decrease weight.

5.2.2 Additional Measurement Opportunities

One very interesting application of this technique would be volume calculation. Given that the technique produces stacked width and length measurements, these could be used to produce an estimated volume for the sample. An additional measurement opportunity is correlating laser penetration depth to root complexity. Figure 47 shows the laser penetration depth measurement.

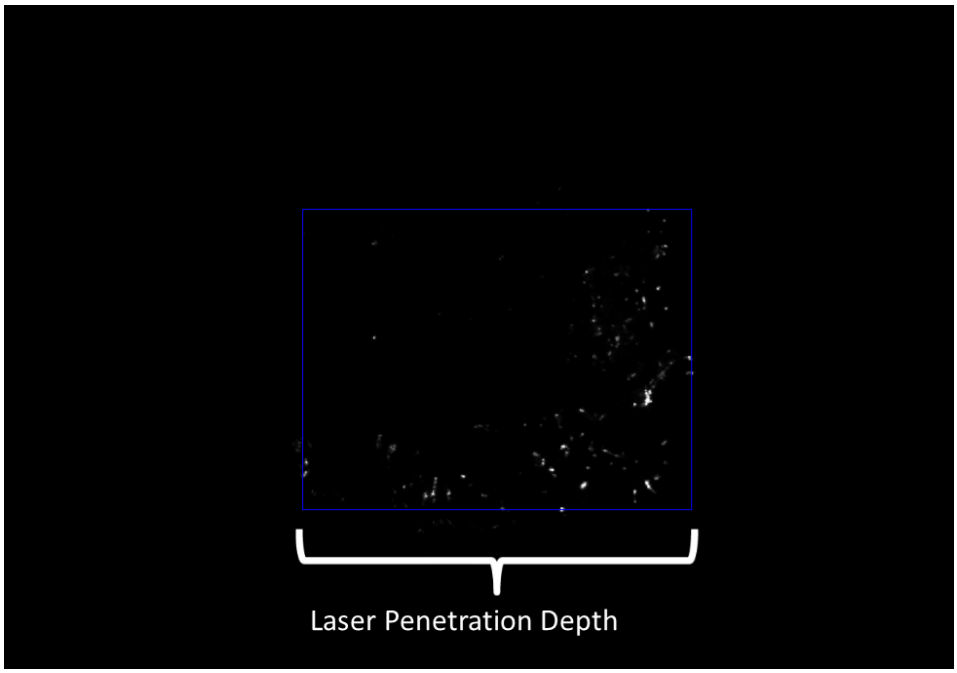

Figure 47: Laser Penetration Depth

Additionally, the technique described above can also be coupled with additional measurement techniques to determine other parameters needed for phenotyping. For example, for corn ears, additional cameras could be mounted at various angles to allow counting kernels, counting the number of rows in the ear, and the length of the barren ear section. Scales could also be mounted in the base to measure the weight of the sample.

This laser measurement technique can be applied to phenotyping other crops. It can be applied via the box method used in this thesis for samples of comparatively small volume (ie produce, seedlings, etc.). The sampling apparatus can be scaled up or down to allow visualization of crop elements of various sizes.

An additional opportunity to utilize this technique involves placing the laser system on a mobile platform such as a robotic arm. The additional degrees of freedom provided by a robotic

arm would allow the laser sheet to illuminate other perspectives of the sample while simultaneously providing information about the end effector's (in this case the laser sheet's) location.

REFERENCES

Abdullah, M. Z., J. Mohamad Saleh, A. S. Fathinul Syahir and B. M. N. Mohd-Azemi. 2006. Discrimination and classification of fresh-cut starfruits (Averrhoa carambola L.) using automated machine vision system. *Journal of Food Engineering* 76(4): 506-523.

Adamchuk, V. I. 2001. Application of a strain gauge array to estimate soil mechanical impedance on-the-go. *Transactions of the ASABE* 44(6): 1377-1383.

Andrade, P. 2004. Field evaluation of the improved version of the UCDavis compaction profile sensor (UCD-CPS). *ASAE Annual International Meeting 2004*265-276.

Armengaud, P., K. Zambaux, A. Hills, R. Sulpice, R. Pattison, M. Blatt and A. Amtmann. 2009. EZ-Rhizo: integrated software for the fast and accurate measurement of root system architecture. *Plant journal* 57(5): 945-956.

Backhaus, A., A. Kuwabara, M. Bauch, N. Monk, G. Sanguinetti and A. Fleming. 2010. leafprocessor: a new leaf phenotyping tool using contour bending energy and shape cluster analysis. *New Phytologist* 187(1): 251-261.

Basu, P. and A. Pal. 2012. A new tool for analysis of root growth in the spatio-temporal continuum. *New Phytologist* 195(1): 264-274.

Basu, S. and A. Alavi. 2011. SPECT-CT and PET-CT in oncology - An overview. *Current Medical Imaging Reviews* 7(3): 202-209.

Batranin, A. V., S. V. Chakhlov, D. V. Grinev, B. I. Kapranov and V. A. Klimenov. 2013. Design of the X-ray micro-CT scanner TOLMI-150-10 and its perspective application in non-destructive evaluation. *Applied Mechanics and Materials* 3793-10.

Berkhout, A. J. 1989. A Unified Approach to Ultrasonic Imaging. In *Non-Destructive Testing,* 9-18. ed. J. Boogaard and G.M. van Dijk, Oxford: Elsevier.

Blasioli, S., E. Biondi, I. Braschi, U. Mazzucchi, C. Bazzi and C. E. Gessa. 2010. Electronic nose as an innovative tool for the diagnosis of grapevine crown gall. *Analytica Chimica Acta* 672(1–2): 20-24.

Brenner, C., C. Dold and N. Ripperda. 2008. Coarse orientation of terrestrial laser scans in urban environments. *ISPRS Journal of Photogrammetry & Remote Sensing* 63(1): 4-18.

Buzug, T. M. 2008. *Computed Tomography From Photon Statistics to Modern Cone-Beam CT*. Berlin: Springer.

Cierniak, R. 2011. *X-Ray Computed Tomography in Biomedical Engineering.* London: Springer.

Clark, C. J., J. S. MacFall and R. L. Bieleski. 1998. Loss of watercore from 'Fuji' apple observed by magnetic resonance imaging. *Scientia Horticulturae* 73(4): 213-227.

Clark, R. T., A. N. Famoso, K. Zhao, J. E. Shaff, E. J. Craft, C. D. Bustamante, S. R. Mccouch, D. J. Aneshansley And L. V. Kochian. 2013. High-throughput two-dimensional root system phenotyping platform facilitates genetic analysis of root growth and development. *Plant, Cell & Environment* 36(2): 454-466.

Cobb, J., G. DeClerck, A. Greenberg, R. Clark and S. McCouch. 2013. Next-generation phenotyping: requirements and strategies for enhancing our understanding of genotype–phenotype relationships and its relevance to crop improvement. *Theoretical and Applied Genetics* 126(4): 867-887.

Costa, C., F. Antonucci, F. Pallottino, J. Aguzzi, D. Sun and P. Menesatti. 2011. Shape Analysis of Agricultural Products: A Review of Recent Research Advances and Potential Application to Computer Vision. *Food and Bioprocess Technology* 4(5): 673-692.

Dais, P. and E. Hatzakis. 2013. Quality assessment and authentication of virgin olive oil by NMR spectroscopy: A critical review. *Analytica Chimica Acta* 7651-27.

De, N., N. De Belie, D. K. Pedersen, M. Martens, R. Bro, L. Munck and J. De Baerdemaeker. 2003. The Use of Visible and Near-Infrared Reflectance Measurements to assess Sensory Changes in Carrot Texture and Sweetness during Heat Treatment. *Biosystems engineering* 85(2): 213-225.

Delwiche, S. R. 1996. Quality characteristics in rice by near-infrared reflectance analysis of whole-grain milled samples. *Cereal Chemistry* 73(2): 257-263.

Ehsani, M. R., S. K. Upadhyaya, D. Slaughter, S. Shafii and M. Pelletier. 1999. A NIR Technique for Rapid Determination of Soil Mineral Nitrogen. *Precision Agriculture* 1(2): 217-234.

ElMasry, G., S. Cubero, E. Moltó and J. Blasco. 2012. In-line sorting of irregular potatoes by using automated computer-based machine vision system. *Journal of Food Engineering* 112(1–2): 60-68.

Fang, G., J. Y. Goh, M. Tay, H. F. Lau and S. F. Y. Li. 2013. Characterization of oils and fats by 1H NMR and GC/MS fingerprinting: Classification, prediction and detection of adulteration. *Food Chemistry* 138(2–3): 1461-1469.

Fang, S., X. Yan and H. Liao. 2009. 3D reconstruction and dynamic modeling of root architecture in situ and its application to crop phosphorus research. *The Plant Journal* 60(6): 1096-1108.

Garbout, A., L. J. Munkholm and S. B. Hansen. 2013. Temporal dynamics for soil aggregates determined using X-ray CT scanning. *Geoderma* 204-20515-22.

Garcia-Ruiz, F. 2013. Comparison of two aerial imaging platforms for identification of Huanglongbing-infected citrus trees. *Computers and Electronics in Agriculture* 91106-115.

Goldratt, E. M. 1990. *What is this thing called theory of constraints and how should it be implemented?* 1st ed. Croton-on-Hudson, N. Y: North River Press.

Gonzalez, Y., Y. González Martín, J. Luis Pérez Pavón, B. Moreno Cordero and C. García Pinto. 1999. Classification of vegetable oils by linear discriminant analysis of Electronic Nose data. *Analytica Chimica Acta* 384(1): 83-94.

Grift, T., Q. Zhang, N. Kondo and K. C. Ting. 2008. A review of automation and robotics for the bio-industry. *Journal of Biomechatronics Engineering* 137-54.

Grift, T. E. 2011. High-throughput phenotyping technology for maize roots. *Biosystems engineering* 110(1): 40-48.

Grift, T. E. 2006. Development of low-cost, root collar diameter measurement devices for pine seedlings. *Computers and Electronics in Agriculture* 52(1-2): 60-70.

Grift, T. E., M. Z. Tekeste and R. R. Raper. 2005. Acoustic compaction layer detection. *Transaction of the ASAE* 481-8.

Grift, T. and M. Bohn. 2013. Maize Root Matters. *Resource Magazine*.

Hak-Jin Kim, J. W. Hummel, K. A. Sudduth and P. P. Motavalli. 2007. Simultaneous Analysis of Soil Macronutrients Using Ion-Selective Electrodes. *Soil Science Society of America Journal* 71(6): 1867-1877.

Heikkilä, J. 1997. Four-step camera calibration procedure with implicit image correction. *Proceedings of the IEEE Computer Society Conference on Computer Vision and Pattern Recognition*1106-1112.

Hernández Gómez, A., J. Wang, G. Hu and A. García Pereira. 2007. Discrimination of storage shelf-life for mandarin by electronic nose technique. *LWT - Food Science and Technology* 40(4): 681-689.

Hsieh, J. 2009. *Computed tomographyprinciples, design, artifacts, and recent advances.* 2nd ed. Bellingham, Wash.: .

Huang, Y., F. Li, Y. Xia and K. Chen. 2011. Scent profiling of Cymbidium ensifolium by electronic nose. *Scientia Horticulturae* 128(3): 306-310.

Hulse, J. H. 2004. Biotechnologies: past history, present state and future prospects. *Trends in Food Science & Technology* 15(1): 3-18.

Jauhar, P. P. 2001. Genetic engineering and accelerated plant improvement: Opportunities and challenges. *Plant cell, tissue and organ culture* 64(2/3): 87-91.

Jiang, N., W. Yang, L. Duan, X. Xu, C. Huang and Q. Liu. 2012. Acceleration of CT reconstruction for wheat tiller inspection based on adaptive minimum enclosing rectangle. *Computers and Electronics in Agriculture* 85123-133.

Kapoulas, V. M. and N. K. Andrikopoulos. 1987. Detection of virgin olive oil adulteration with refined oils by second-derivative spectrophotometry. *Food Chemistry* 23(3): 183-192.

Koc, A. 2012. Canũelo, A., Garcia-Reyes, J.F., Molina-Diaz, A., Trojanowicz, M. Low-molecular weight protein profiling of genetically modified maize using fast liquid chromatography electrospray ionization and time-of-flight mass spectrometry. *Journal of separation science* 35(12): 1447-1461.

Korostynska, O., R. Blakey, A. Mason and A. Al-Shamma'a. 2013 Novel method for vegetable oil type verification based on real-time microwave sensing. *Sensors and Actuators A: Physical*.

Kotwaliwale, N., A. Kalne and K. Singh. 2012. Monitoring of mango (Mangifera indica L.) (Cv.: Chousa) ripening using X-ray computed tomography. In *Proceedings of the International Conference on Sensing Technology, ICST*, 326-330.

Lauterbur, P. C. 1973. Image formation by induced local interactions: Examples employing nuclear magnetic resonance. *Nature* 242(5394): 190-191.

Lee, K. and B. Lee. 2013. Estimation of rice growth and nitrogen nutrition status using color digital camera image analysis. *European Journal of Agronomy* 4857-65.

Leemans, V., H. Magein and M. -. Destain. 1998. Defects segmentation on 'Golden Delicious' apples by using colour machine vision. *Computers and Electronics in Agriculture* 20(2): 117-130.

Liming, X. and Z. Yanchao. 2010. Automated strawberry grading system based on image processing. *Computers and Electronics in Agriculture* 71(SUPPL. 1): S32-S39.

Liu, C., B. Chen, Y. Liu and T. Zha. 2012. Quantity Detection of Kernels in an Ear Corn Based on Machine Vision. *Applied mechanics and materials* 246-247279-285.

Longuetaud, F., J. -. Leban, F. Mothe, E. Kerrien and M. -. Berger. 2004. Automatic detection of pith on CT images of spruce logs. *Computers and Electronics in Agriculture* 44(2): 107-119.

Mahlein, A., Rumpf, T., Welke, P. -. Dehne, H., Plümer, L., Steiner, U., and Oerke E., 2013. Development of spectral indices for detecting and identifying plant diseases. *Remote Sensing of Environment* 12821-30.

Manickavasagan, A., G. Sathya, D. S. Jayas and N. D. G. White. 2008. Wheat class identification using monochrome images. *Journal of cereal science* 47(3): 518-527.

Mansfield, P. and I. L. Pykett. 1978. Biological and medical imaging by NMR. *Journal of Magnetic Resonance* 29355-373.

Martens, M. 1986. Near-Infrared Reflectance Determination of Sensory Quality of Peas. *Applied Spectroscopy* 40(3): 303-310.

Mason, W. and Thurston, R. 1975. *Physical acoustics: principles and methods.* New York: New York, Academic Press.

Mees, F., R. Swennen, M. Van Geet and Jacobs P. 2003. Applications of X-ray Computed Tomography in the Geosciences. *Geological Society Special Publication.* 21510/14/2013-1-6.

Merbach, A., L. Helm and É. Tóth, eds. 2013. *The Chemistry of Contrast Agents in Medical Magnetic Resonance Imaging.* 2nd ed. Chichester, West Sussex: Wiley.

Molina, R., C. Aguilar, A. Pacheco, A. Cruz Orea and M. Canseco. 2013. Alternative Method to Characterize Corn Grain by Means of Photoacoustic Spectroscopy. *International Journal of Thermophysics*1-9.

Mooney, S. J., Morris, C., Berry P.M., 2006. Visualization and quantification of the effects of cereal root lodging on three-dimensional soil macrostructure using x-ray computed tomography. *Soil Science* 171(9): 706-718.

Neethirajan, S., D. S. Jayas, N. D. G. White and H. Zhang. 2008. Investigation of 3D geometry of bulk wheat and pea pores using X-ray computed tomography images. *Computers and Electronics in Agriculture* 63(2): 104-111.

Newman, P., G. Rozycki,, 1998. The History of Ultrasound. *The Surgical clinics of North America* 78(2): 179-195.

Nielsen, R. L. 2012. Historical Corn Grain Yields for Indiana and the U.S. Available at: http://www.agry.purdue.edu/ext/corn/news/timeless/YieldTrends.html. Accessed May 23 2013.

Núñez Andrés, M. A. and F. Buill Pozuelo. 2009. Evolution of the architectural and heritage representation. *Landscape and Urban Planning* 91(2): 105-112.

Ophir, R. 2013. Bioinformatics tools for marker discovery in plant breeding. *Israel Journal of Chemistry* 53(3-4): 173-179.

Osswald, S., A. Hornung and M. Bennewitz. 2012. Improved proposals for highly accurate localization using range and vision data. In *IEEE International Conference on Intelligent Robots and Systems*, 1809-1814.

Parayil, G. 2003. Mapping technological trajectories of the Green Revolution and the Gene Revolution from modernization to globalization. *Research Policy* 32(6): 971-990.

Peleman, J. D., J.R. Van Der Voort, 2003. Breeding by design. *Trends in plant science* 8(7): 330-334.

Pérez-de-Castro, A.M., S. Vilanova, J. Cañizares, L. Pascual, J.M. Blanca, M.J. Díez, J. Prohens, B. Picó. 2012. Application of genomic tools in plant breeding. *Current Genomics* 13(3): 179-195.

Popescu, S. C. Wynne, R.H., Nelson, R.F. 2003. Measuring individual tree crown diameter with lidar and assessing its influence on estimating forest volume and biomass. *Canadian journal of remote sensing* 29(5): 564-577.

Roh, H. C., C. H. Sung and M. J. Chung. 2013. Rapid SLAM using simple map representation in indoor environment. In *FCV 2013 - Proceedings of the 19th Korea-Japan Joint Workshop on Frontiers of Computer Vision*, 225-229.

Romano, G., S. Zia, W. Spreer, C. Sanchez, J. Cairns, J. L. Araus and J. Müller. 2011. Use of thermography for high throughput phenotyping of tropical maize adaptation in water stress. *Computers & Electronics in Agriculture* 79(1): 67-74.

Romeo, J., J. Guerrero, M. Montalvo, L. Emmi, M. Guijarro, P. Gonzalez-de-Santos and G. Pajares. 2013. Camera Sensor Arrangement for Crop/Weed Detection Accuracy in Agronomic Images. *Sensors* 13(4): 4348-4366.

Samseemoung, G., P. Soni, H. P. W. Jayasuriya and V. Salokhe. 2012. Application of low altitude remote sensing (LARS) platform for monitoring crop growth and weed infestation in a soybean plantation. *Precision agriculture* 13(6): 611-627.

Santamaría, J., O. Cordón, S. Damas, J. M. García-Torres and F. Navarro. 2011. A study of the suitability of evolutionary computation in 3D modeling of forensic remains. *Lecture Notes in Computer Science (including subseries Lecture Notes in Artificial Intelligence and Lecture Notes in Bioinformatics)* 7023 LNAI293-302.

Schwarzschild, B. 2003. Lauterbur and Mansfield Awarded Nobel Medicine Prize for Magnetic Resonance Imaging. *Physics Today* 56(12): 24-27.

Se, S. and P. Jasiobedzki. 2006. Photo-realistic 3D model reconstruction. *Proceedings 2006 IEEE International Conference on Robotics and Automation, 2006. ICRA 2006.* 20063076-3082.

Severini, A. D., L. Borrás and A. G. Cirilo. 2011. Counting Maize Kernels through Digital Image Analysis. *Crop Science* 51(6): 2796-2800.

Sholts, S.B. , S.K.T.S. Wärmländer, L.M. Flores, K.W.P. Miller, and P.L. Walker. 2010. Variation in the Measurement of Cranial Volume and Surface Area Using 3D Laser Scanning Technology. *Journal of forensic sciences* 55(4): 871-876.

Sinfield, J. V., D. Fagerman and O. Colic. 2010. Evaluation of sensing technologies for on-the-go detection of macro-nutrients in cultivated soils. *Computers and Electronics in Agriculture* 70(1): 1-18.

Tamas, L., and L.C. Goron. 2012. 3D map building with mobile robots. *2012 20th Mediterranean Conference on Control Automation (MED)*134-139.

Tang, P. and B. Akinci, 2012. Formalization of workflows for extracting bridge surveying goals from laser-scanned data. *Automation in Construction* 22(0): 306-319.

Tsai, R. 1987. A versatile camera calibration technique for high-accuracy 3d machine vision metrology using off-the-shelf tv cameras and lenses. *IEEE Journal of Robotics and Automation* 3(4): 323-344.

Turkan, Y., F. Bosché, Haas, C.T, and Haas, R. 2013. Toward Automated Earned Value Tracking Using 3D Imaging Tools. *Journal of Construction Engineering and Management* 139(4): 423-433.

Ulukan, H. 2009. The evolution of cultivated plant species: classical plant breeding versus genetic engineering. *Plant Systematics & Evolution* 280(3): 133-142.

Van der Zande, D., Hoet, W., Jonckheere, I., van Aardt, J., and Coppin, P. 2006. Influence of measurement set-up of ground-based LiDAR for derivation of tree structure. *Agricultural and Forest Meteorology* 141(2–4): 147-160.

Vaughan, D. A., Balazs E., and Heslop-Harrison, J. S.. 2007. From Crop Domestication to Super-domestication. *Annals of botany* 100(5): 893-901.

Welle, R., W. Greten, T. Müller, G. Weber and H. Wehrmann. 2005. Application of near infrared spectroscopy on-combine in corn grain breeding. *Journal of Near Infrared Spectroscopy* 13(2): 69-75.

Xiong, X., A. Adan, B. Akinci and D. Huber. 2013. Automatic creation of semantically rich 3D building models from laser scanner data. *Automation in Construction* 31325-337.

Yoshida, K., E. Ishikawa, M. Joshi, H. Lechat, F. Ayouni and M. Bonnefille. 2012. Quality Control and Rancidity Tendency of Nut Mix Using an Electronic Nose. *Perception and Machine Intelligence* 7143163-170.

Yu, L. and D. Qi. 2008. Analysis and processing of decayed log CT image based on multifractal theory. *Computers and Electronics in Agriculture* 63(2): 147-154.

Zeder, M. A. 2011. The Origins of Agriculture in the Near East. *Current anthropology* 52(S4, The Origins of Agriculture: New Data, New Ideas): S221-S235.

Zhang, H. and J. Wang. 2007. Detection of age and insect damage incurred by wheat, with an electronic nose. *Journal of stored products research* 43(4): 489-495.

Zhang, L. and T. E. Grift. 2012. A LIDAR-based crop height measurement system for Miscanthus giganteus. *Computers and Electronics in Agriculture* 8570-76.

Zhang, L. and T. E. Grift. 2012. A monocular vision-based diameter sensor for Miscanthus giganteus. *Biosystems Engineering* 111(3): 298-304.

Zhang, N. and C. Chaisattapagon. 1995. Effective criteria for weed identification in wheat fields using machine vision. *Transactions of the ASABE* 38(3): 965-974.

Zhu, J., P. A. Ingram, P. N. Benfey and T. Elich. 2011. From lab to field, new approaches to phenotyping root system architecture. *Current opinion in plant biology* 14(3): 310-317.

APPENDIX A: IMAGING BOX CONTROL SOFTWARE

```
% Laser movement (BD1)
% 1000 pulses, half stepped, is about 5 inches (127mm)
% Total movement needed is approx. 2000 pulses = 254 mm

% Root rotation (BD2)
% The stepper motor has 400 Pulses Per Revolution (PPR), in other words,
% 1 pulse -> 0.9 deg. % II100 -> 90 deg, II200 -> 180 deg. Negative is CCW.
%
% The board address can be programmed by connecting it directly to a COM port,
% and using the program SetAddress_STP101.m

clear all;
close all;
clc;

%================================  Constants  ============================
VertDistMax          = 254;                 %mm, used for warning
PortNr               = 0;
RotAngle             = 0;
VertSpacing          = 0;
NrVertSteps          = 0;

Puls2Height          = 127/1000;            % mm  / puls
Puls2Rotation        = 360/400;             % deg / puls

DelayLaser           = 1;                   % s, Give camera time to take a
shot
DelayRoot            = 1;                   % s, Give root time to stabilize
after turning
NrVerticalSteps      = 20;                  % number of steps up

%================ Vertical Spacing user input ============================
while VertSpacing  < 0.1 || VertSpacing > 100
   VertSpacing   = round(input('Enter vertical spacing in mm: '));
end
NrPulsesVertical = round(VertSpacing / Puls2Height);
disp(['True vertical spacing = ' num2str(NrPulsesVertical*Puls2Height) ' mm =
'  num2str(NrPulsesVertical) ' pulses'])
disp(' ')

%================ Nr vertical steps user input ===========================
while NrVertSteps  < 1 || NrVertSteps > 360
   NrVertSteps    = round(input('Enter number of vertical steps: '));
   TotalVertDist  = NrVertSteps*NrPulsesVertical*Puls2Height;
   disp(['Total vertical distance = ' num2str(TotalVertDist) ' mm'])
   if TotalVertDist > VertDistMax
      warndlg(['Total vertical distance of ' num2str(TotalVertDist) ' >
Maximum of ' num2str(VertDistMax) ])
   end
   disp(' ')
end
```

```
%================ Rotational angle user input ==========================
while RotAngle  < 1 || RotAngle > 360
   RotAngle    = round(input('Enter rotational angle in degrees: '));
end
NrPulsesRotational    = round(RotAngle / Puls2Rotation);
disp(['True rotational angle = ' num2str(NrPulsesRotational*Puls2Rotation) '
deg = '  num2str(NrPulsesRotational) ' pulses'])
disp(' ')
NrRotations = round(360/RotAngle);

%======================== COM port user input ==========================
while PortNr < 1 || PortNr > 12
   PortNr    = round(input('Enter COM port (1-8): '));
end

%======================== Attempt opening COM ==========================
try
   eval(['SerialPort = serial(''COM' num2str(PortNr) ''');']);

set(SerialPort,'Baudrate',9600,'Databits',8,'Parity','none','StopBits',1,'Ter
minator','CR');
   fopen(SerialPort);
   disp(['Opening COM' num2str(PortNr)])
   pause(1)
catch COMportException
   disp(['COM' num2str(PortNr) ' not available, check Control Panel.'])
   pause(1)
end
disp(' ')

%============================ Initialize TopCamera =====================
imaqreset;

TopCamera     = videoinput('dcam', 1,'Y8_1280x960');
triggerconfig(TopCamera, 'manual');
set(TopCamera,'framespertrigger', 1);
set(TopCamera,'TriggerRepeat', inf);

%======================== Initialize stepper motors ====================
fprintf(SerialPort,'BD1')     % Board select is 1 (Laser movement)
fprintf(SerialPort,'CR')

fprintf(SerialPort,'SO')      % Power off prolongs motor life
fprintf(SerialPort,'CR')

fprintf(SerialPort,'SH')      % Half step
fprintf(SerialPort,'CR')

fprintf(SerialPort,'BD2')     % Board select is 2 (Root rotation)
fprintf(SerialPort,'CR')

fprintf(SerialPort,'SO')      % Power off prolongs motor life
fprintf(SerialPort,'CR')
```

```
fprintf(SerialPort,'SH')      % Half step
fprintf(SerialPort,'CR')

FileName             = input('Enter filename','s');

YN = input('Place root in imaging system, turn laser on, hit Enter when
ready');
for i = 1:(NrRotations)
   for j = 1:NrVerticalSteps
      start(TopCamera);
      trigger(TopCamera);
      L_image  = getdata(TopCamera,1);
      imwrite(L_image,[num2str(FileName) '_'  num2str(90*(i-1)) '_' num2str(j)
'.tif'],'tif');
      stop(TopCamera);

      fprintf(SerialPort,'BD1')     % Board select is 1 (Laser movement)
      fprintf(SerialPort,'CR')
      fprintf(SerialPort,['II' num2str(NrPulsesVertical)]');
      fprintf(SerialPort,'CR');
      pause(DelayLaser);            % s, Give camera time to take a shot
   end

   % Return laser to original position
   fprintf(SerialPort,'BD1')
   fprintf(SerialPort,'CR')
   fprintf(SerialPort,['II' num2str(-NrVerticalSteps*NrPulsesVertical)]');
   fprintf(SerialPort,'CR');

   % Rotate root through RotAngle degrees
   fprintf(SerialPort,'BD2')        % Board select is 2 (Root rotation)
   fprintf(SerialPort,'CR')
   fprintf(SerialPort,['II' num2str(NrPulsesRotational)]');
   fprintf(SerialPort,'CR');
   pause(DelayRoot)
end

% If the program is interrupted by CTRL-C, make sure to run this line to
close
% the serial port, otherwise MatLab needs to be restarted.
fclose(SerialPort);
disp(['Closing COM' num2str(PortNr)])
```

APPENDIX B: IMAGE PROCESSING SOFTWARE

The image processing software consists of two pieces of software: a batch program named LaserRootAngleBatch and an additional program named LaserRootAngle. Both can be found below.

LaserRootAngleBatch:

```
%[DataFileName,DataFilePath]    = uigetfile('*.xls', 'Select Root Data File
');
DataFileName = 'RootData1.xlsx';
DataFilePath = 'C:\CORNLASER3\Sample_Images_New\';

if ~isequal(DataFileName,0) && ~isequal(DataFilePath,0);
   DataChannel  = ddeinit('excel',DataFileName);
   if DataChannel == 0                                          % dde link NOT
established
      msgbox(['Open ' DataFileName ' in Excel'],'Excel link','warn')
   else
      ChannelActive  = 1;
   end
end

ddepoke(DataChannel,['r1c2:r1c2'],'Width,  0',[1 1]);
ddepoke(DataChannel,['r1c3:r1c3'],'Width, 90',[1 1]);
ddepoke(DataChannel,['r1c4:r1c4'],'Width,180',[1 1]);
ddepoke(DataChannel,['r1c5:r1c5'],'Width,270',[1 1]);

ddepoke(DataChannel,['r1c6:r1c6'],'Height,  0',[1 1]);
ddepoke(DataChannel,['r1c7:r1c7'],'Height, 90',[1 1]);
ddepoke(DataChannel,['r1c8:r1c8'],'Height,180',[1 1]);
ddepoke(DataChannel,['r1c9:r1c9'],'Height,270',[1 1]);

Orient         = [0;90;180;270];


for RootNr = 17:17
   RowOffSet = (RootNr-1) * 22
   RootMatW  = zeros(20,4);
   RootMatH  = zeros(20,4);
   for View = 1:4;
      for LaserLevel = 1:20
         if RootNr > 9
            FileName = [num2str(RootNr) '_' num2str(Orient(View)) '_'
num2str(LaserLevel) '.tif']
```

```
         else
            FileName = ['0' num2str(RootNr) '_' num2str(Orient(View)) '_'
num2str(LaserLevel) '.tif']
         end
         ddepoke(DataChannel,['r' num2str(RowOffSet+1) 'c1:r'
num2str(RowOffSet+1) 'c1'],['RootNr: ' num2str(RootNr)],[1 1]);
         [Width, Height, threshold] = LaserRootAngle([DataFilePath FileName]);
         %ddepoke(DataChannel,['r' num2str(RowOffSet+(LaserLevel+1)) 'c1:r'
num2str(RowOffSet+(LaserLevel+1)) 'c1'],LaserLevel,[1 1]);
         ddepoke(DataChannel,['r' num2str(RowOffSet+(LaserLevel+1)) 'c1:r'
num2str(RowOffSet+(LaserLevel+1)) 'c1'],threshold,[1 1]);
         ddepoke(DataChannel,['r' num2str(RowOffSet+(LaserLevel+1)) 'c'
num2str(View+1) ':r' num2str(RowOffSet+(LaserLevel+1)) 'c'
num2str(View+1)'],Width,[1 1]);
         ddepoke(DataChannel,['r' num2str(RowOffSet+(LaserLevel+1)) 'c'
num2str(View+5) ':r' num2str(RowOffSet+(LaserLevel+1)) 'c'
num2str(View+5)'],Height,[1 1]);
      end
   end
end

ddeterm(DataChannel)
```

LaserRootAngle

```
% Function  : Compute RootAngles from laser intercept images


function [Width, Height, threshold] = LaserRootAngle(filelocation)

if nargin == 0
   close all
   clear all
   clc
   [filename,path]= uigetfile('*.tif', 'Open TIF Imagefile ');
   filelocation = [path, filename];
   ShowImage = 1;
else
   ShowImage = 0;
end

clear Width Height
close all
clc

%====================              CODE              ====================
RootImage         = imread(filelocation);
%[H,W]             = size(RootImage);

%if ShowImage
%   figure, imshow(RootImage)
```

```
%end

% Threshold the image
%threshold         = graythresh(RootImage)

threshold         = 0.3;
BW                = im2bw(RootImage,threshold);

if mean(mean(BW)) > 0;
   [p_L,q_L] = find(BW > 0.5);

   % if ShowImage
   figure, imshow(BW)
   % end

   line([min(q_L), max(q_L)],[min(p_L), min(p_L)]) % Top line
   line([min(q_L), min(q_L)],[min(p_L), max(p_L)]) % Left line
   line([max(q_L), max(q_L)],[min(p_L), max(p_L)]) % Right line
   line([max(q_L), min(q_L)],[max(p_L), max(p_L)]) % Bottom line

   Height = max(p_L) - min(p_L);
   Width  = max(q_L) - min(q_L);
   pause(0.1)
else
   disp('Image has no data')
   Height = 0;
   Width  = 0;
end
```